Tectonophysics 755 (2019) 109–126

Contents lists available at ScienceDirect

Tectonophysics

journal homepage: www.elsevier.com/locate/tecto

Crustal P wave velocity structure beneath the SE margin of the Tibetan Plateau from Deep Seismic Sounding results

Jiyan Lin[a,b,c], Walter D. Mooney[d], Fuyun Wang[c,*], Yonghong Duan[c], Xiaofeng Tian[c], Tao Xu[a,e], Youguo Deng[f]

[a] State Key Laboratory of Lithospheric Evolution, Institute of Geology and Geophysics, Chinese Academy of Sciences, Beijing 100029, China
[b] University of Chinese Academy of Sciences, Beijing 100049, China
[c] Geophysical Exploration Center, China Earthquake Administration, Zhengzhou 450002, China
[d] U. S. Geological Survey, Menlo Park, CA 94025, USA
[e] CAS Center for Excellence in Tibetan Plateau Earth Sciences, Beijing 100101, China
[f] China University of Geosciences, Wuhan 430074, China

ARTICLE INFO

Keywords:
SE margin Tibet
Deep Seismic Sounding
P-wave velocity structure
Lower crustal flow
Deep processes

ABSTRACT

The crust and uppermost mantle beneath the southeastern (SE) margin of Tibetan Plateau record the lateral expansion of Tibet and far-field effects from the ongoing continental collision and convergence. In order to obtain constraints on the deep structure and the eastward expansion of the plateau, we synthesized Deep Seismic Sounding (DSS) results in this region and constructed the P wave velocity models for each terrane. The principal characteristics of the crustal velocity model and tectonic significance are: (1) Crustal thickness decreases from 53 km beneath the Songpan-Ganzi terrane (SGT) to 34 km in the south direction beneath Simao terrane (SMT), and 42 km in the east direction beneath Chengdu area. The crust is dominantly felsic in upper crust, with a small percentage of mafic composition in the lower crust. (2) The crustal structure is very heterogeneous in this region. The Indochina Block is characterized by low seismic velocities in the upper crust, while the west Yangtze terrane (WYZT) and SGT show higher velocities in the upper crust. The lower crust beneath WYZT is relatively thicker than other terranes. (3) We deduce that the high velocity in the upper crust and relatively thick lower crust beneath the SGT and WYZT can be associated with magmatic processes that generated the Emeishan flood basalts which may have been triggered by rifting or mantle plume. The lateral variations of the crustal thickness in SE Tibet may be due to lower crustal flow from the Tibetan Plateau to the SE direction after blocked by the cold and rigid Yangtze craton in the east direction.

1. Introduction

During the past 50 Ma, the collision between the Indian and Eurasian plates has had a profound influence on the surrounding area of the Tibetan Plateau, particularly the southeast of the Tibetan Plateau. Four main models have been proposed to interpret the plateau formation and regional deformation: (1) the lateral extrusion model (Tapponnier et al., 1982), (2) the vertically coherent deformation model (England and Houseman, 1986), (3) the stepwise rise model (Tapponnier et al., 2001) and (4) the lower crustal flow model (Royden et al., 1997; Clark and Royden, 2000; Royden et al., 2008). The topography in this area is highly variable (Fig. 1), ranging from an altitude of nearly 5000 m in the northwest to less than 1000 m in the east and the southeast. Major tectonic features and a geological map are shown in Fig. 2. It is evident that NW-SE and NS trending faults dominate this area. The most significant fault is the Red River fault (RRF), which starts at the east margin of the Tibetan Plateau and extends to the South China Sea, separating the Indochina block and South China (Lei et al., 2009; Zhu et al., 2009). Southwest China has a high level of seismic activity. Some 238 moderate earthquakes (magnitude greater than 6.0) have occurred since 1970, including the Wenchuan Ms. 8.0 earthquake on 12 May 2008. Due to the high seismic hazard, it is vital to define the crustal structure and related geodynamic processes in this area. Here we summarize the crustal P wave velocity structure of different geological units and correlate this information with the tectonic evolution.

From 1982 to 2016, several Deep Seismic Sounding (DSS) profiles were acquired in this region (Fig. 1). In addition, complementary studies, such as surface wave tomography (Sun et al., 2014; Wang et al.,

* Corresponding author.
E-mail address: wfy@gec.ac.cn (F. Wang).

https://doi.org/10.1016/j.tecto.2019.01.010
Received 11 September 2018; Received in revised form 9 January 2019; Accepted 23 January 2019
Available online 26 January 2019
0040-1951/

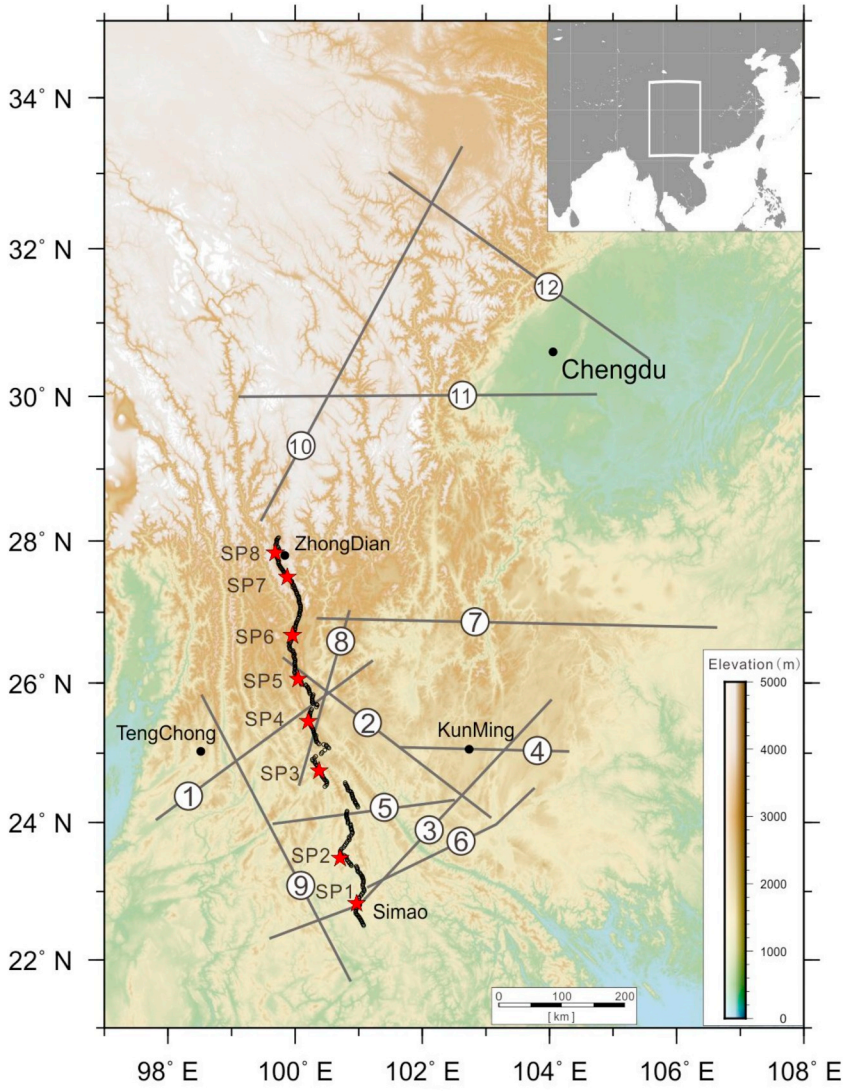

Fig. 1. Location of seismic profiles in the study area. Red stars represent the shot points and black circles represent recording stations. Grey lines indicate the 12 existing DSS profiles: (1) Zhefang-Binchuan [Kan et al., 1986]; (2) Eryuan-Jiangchuan [Kan et al., 1986]; (3) menglian-Malong [Kan et al., 1986]; (4) Chuxiong-Luoping [Wang et al., 2009]; (5) Zhenkang-Luxi [Wang et al., 2014a]; (6) Puer-Luxi [Zhang et al., 2013a]; (7) Lijiang-Qingzhen [Xu et al., 2015]; (8) Yunxian-Ninglang [Chen et al., 2016]; (9) Menghai-Lushui [Wang et al., 2015]; (10) Benzilan-Tangke [Wang et al., 2007]; (11) Zhubalong-Zizhong [Wang et al., 2007]; (12) Suining-Aba [Jia et al., 2014a]. Inset map shows the location of the study area. (For interpretation of the references to color in this figure legend, the reader is referred to the web version of this article.)

2014b; Fu et al., 2017; Li et al., 2017), receiver function inversion (Bai et al., 2010b; Chen et al., 2010; Wang et al., 2017; Yu et al., 2017; Zhang et al., 2017), travel time tomography (Lei et al., 2009, 2014), shear wave splitting (Huang et al., 2007), ambient noise interferometry (Huang et al., 2010), and GPS measurements (Zhang et al., 2004; Shen et al., 2005) have been reported, leading to new insights into the dynamics of southwest China. Low velocity zones (LVZ) and High velocity zones (HVZ) were constrained at different depth by varying geophysical methods, particular at the major faults and tectonically active region, indicating very heterogeneous crust and uppermost mantle. The Simao-Zhongdian DSS profile crosses through three main tectonic units in SE Tibet and these data have a high signal-to-noise ratio, which is valuable for the study of crustal structure. Although these data have been interpreted by previous authors (Lin et al., 1993; Bai and Wang, 2003; Zhang et al., 2006; Zhang and Wang, 2009), there is still some uncertainty regarding the crustal velocity structure. For example, the crustal velocity in the middle and lower crust shows big difference, and the Moho geometry also presents some difference. In addition, they did not give the uncertainty of the Moho depth. For these reasons, we re-pick the travel times, processed the data by 3 common used methods (Raytracing SEIS-83; finite-difference inversions; synthetic seismogram reflectivity) to constrain the model. We also present comparisons with recently published DSS results, summarize the crustal P-wave seismic velocity structure in different geologic terrains, discuss the composition of the crust and tectonic significance in this region. Our re-analysis of these high-quality data are justified by the more comprehensive geologic and tectonic interpretation presented here.

2. Geologic setting

Our study region is mainly divided into four tectonic units: the Indochina block to the southwest, the Yangtze craton and Cathaysian block in the east, and the Songpan-Ganzi terrane to the north (Fig. 2). Situated to the southeast of the Tibetan plateau and connected to the South China Sea, the Indochina block has experienced extrusion and clockwise rotation since 35 Ma (Steckler et al., 2016; Yu et al., 2017). Three secondary terranes, the Tengchong, Baoshan, and Simao terranes, belong to the Indochina block and are separated by two deep faults, namely the Nujiang and Lancangjiang faults (LCJF). Northeast of the Ailaoshan fault and Red River fault, Yangtze craton and Cathaysian block constitute the South China plate, which represents a stable continental region (Calais et al., 2006; Zhang et al., 2009, 2013b). The

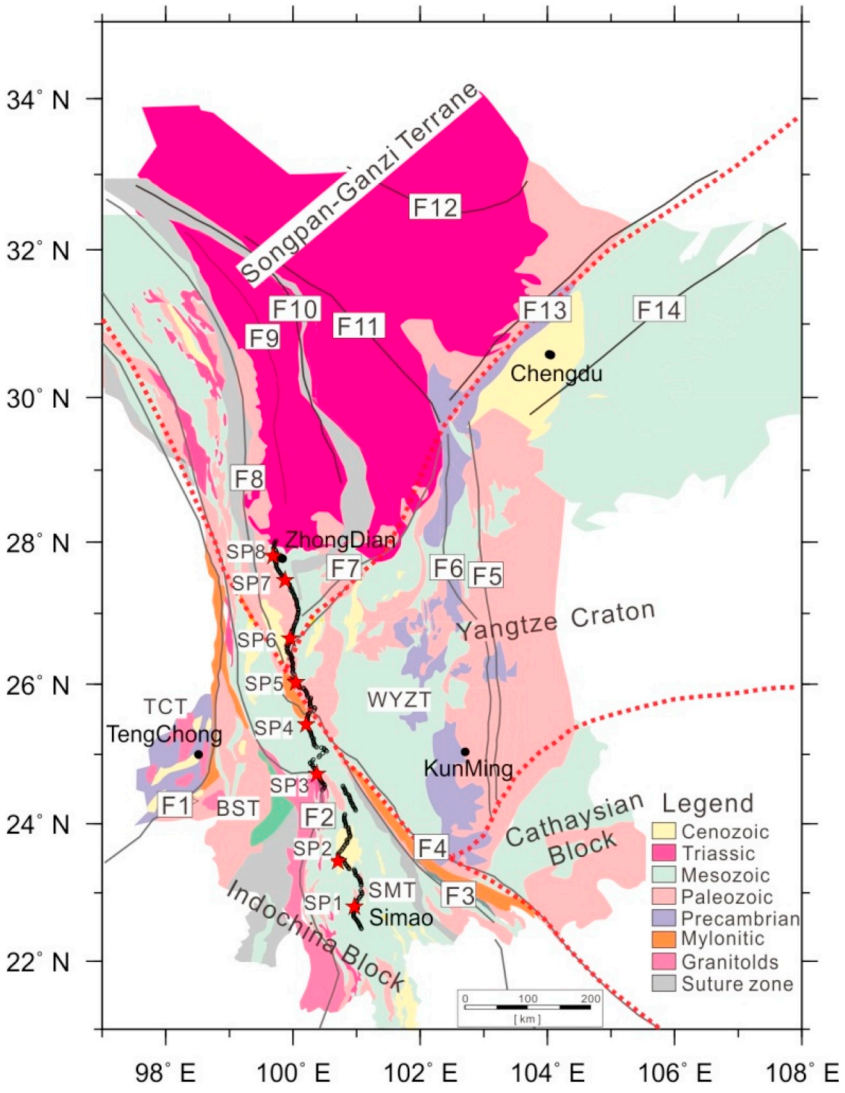

Fig. 2. Tectonic features and Geologic map in the study region (modified from Akciz et al. (2008), Deng et al. (2014b) and Zheng et al. (2017)). The black solid lines and the red dotted lines represent major faults and tectonic division boundaries, respectively. The names of faults and geological units are as follow: F1: Nujiang fault; F2: Lancangjiang fault; F3: Ailaoshan fault; F4: Red River fault; F5: Xiaojiang fault; F6: Anninghe fault; F7: Lijiang-Ninglang fault; F8: Jinshajiang fault; F9: Xiangcheng fault; F10: Ganzi-Litang fault; F11: Xianshuihe fault; F12: Longriba fault; F13: Longmenshan fault; F14: Longquanshan fault; TCT: Tengchong terrane; BST: Baoshan terrane; SMT: Simao terrane; WYZT: Western Yangtze terrane. (For interpretation of the references to color in this figure legend, the reader is referred to the web version of this article.)

Songpan-Ganzi terrane occupies a large part of the eastern Tibetan Plateau, and is bounded by the South China block to the east and the Indochina block to the south.

The Tengchong and Baoshan terranes are land masses separated from the Gondwana supercontinent during the late Paleozoic (400–250 Ma) and have the same characteristics in terms of stratigraphic sequence (Ma, 2002). The Simao terrane is covered by relatively thick Mesozoic-Cenozoic sediments (Fig. 2), without much Precambrian basement and magmatic rock in outcrop. Ophiolite complexes, which are composed of peridotites, gabbros and basalts, were found distributed along the Nujiang, Lancangjiang and Red River faults, representing the closure of the Paleotethyan Ocean (Deng et al., 2014a). Moreover, Mylonitic granite rocks (30–20 Ma), composed by gneisses with amphibolite enclaves, are mainly exposed along these faults, demonstrating that intense deformation exists among these terranes during Cenozoic (Deng et al., 2014b). In the past 5 Ma, Tengchong terrane has experienced some volcanic activity, exhibiting a higher geothermal gradient and numerous hot springs (Lei et al., 2009; Wang, 2001; Zhu et al., 1983).

The Yangtze craton is located in south China and formed during the Archean era. It is surrounded by the North China craton, Tibetan Plateau and Cathaysian block. Proterozoic rocks are widespread in the Yangtze craton, with some Mesozoic-Cenozoic sediments distributed in the west and associated with the Yanshan (200–65 Ma) and Indosinian (250–200 Ma) orogenic movements (Li et al., 2015; Zhang et al., 2009, 2013b; Zheng et al., 2006). Although the Yangtze craton largely stabilized after the Yangtze orogeny (825 Ma), tectonic activity continued to affect the region. Multi-phase magmatism provided large volumes of granite and gneissic granite in the craton, particularly in the western part. The Emeishan Large Igneous Province (LIP) is located in the western margin of the Yangtze craton and the Emeishan basalts are exposed in a scope of 250,000 km^2 formed in late Paleozoic era (250 Ma). (Xu et al., 2001; He et al., 2003; Xu et al., 2015).

The Songpan-Ganzi terrane (SGT), which is a narrow and triangular section in the eastern Tibetan Plateau, is characterized by a thick sequence of Triassic strata of deep marine deposits, at least several kilometers thick, referred to as the Songpan-Ganzi flysch complex (Yin and Harrison, 2000). The SGT has been interpreted as a remnant ocean between the colliding south and north China blocks, a Permian-Triassic rift basin and a back-arc basin (Enkelmann et al., 2007). In the southeastern SGT, where our study was conducted, strata are composed of Triassic deposits and Proterozoic rocks according to the geological map

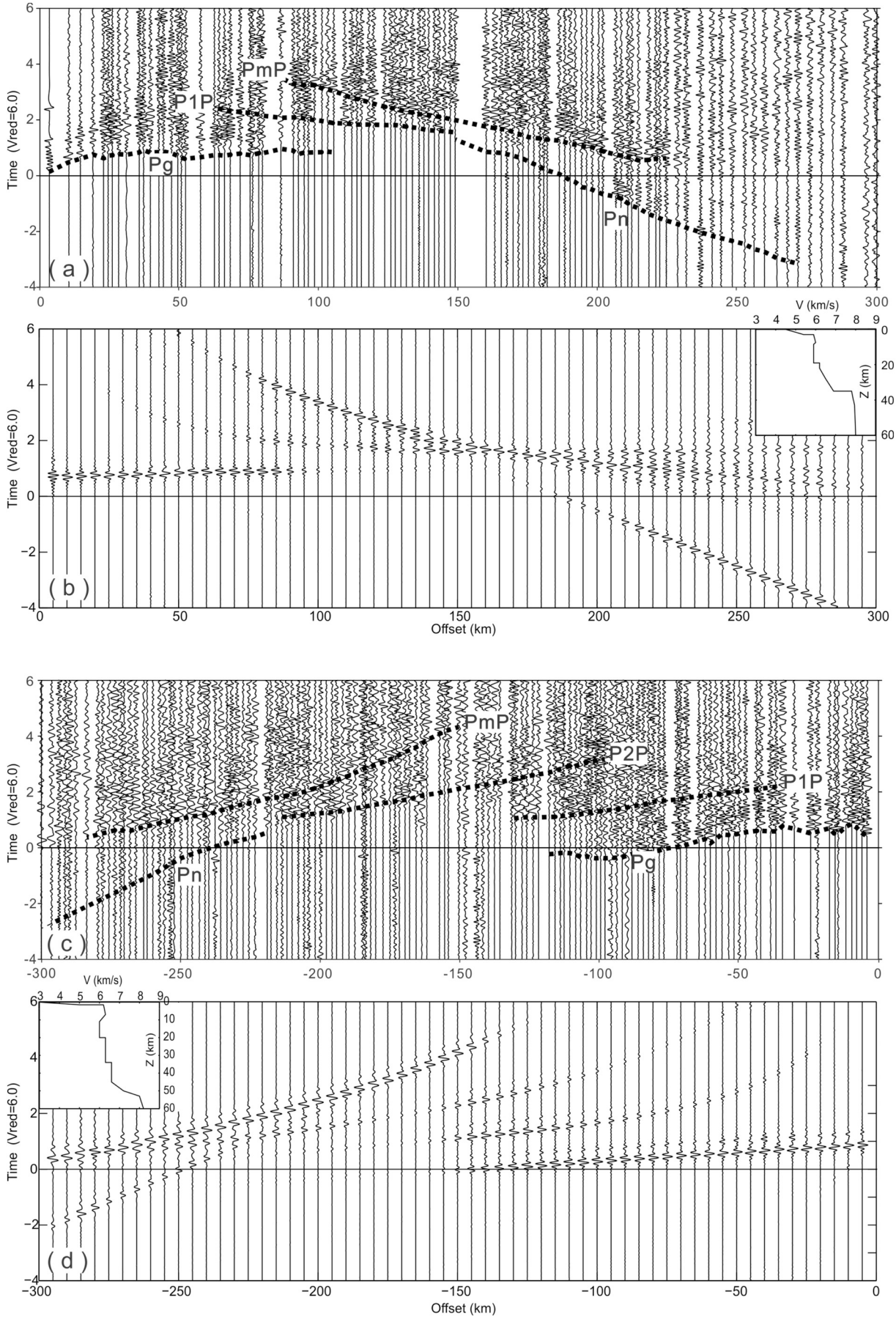

(caption on next page)

Fig. 3. P-wave record sections and associated synthetic seismograms. (a) Shot point 1 (SP1) record section with black dashed lines indicating seismic phases: Pg is the direct phase, P1P is a reflection from the bottom of the crystalline upper crust, PmP is the Moho reflection and Pn is refraction phase from the upper most mantle. (b) Synthetic seismogram record section of SP1 (inset is the corresponding one dimensional (1D) seismic velocity-depth function). (c) Record section of SP8. P2P is a reflection from the bottom of the crystalline middle crust. (d) Synthetic seismogram record section of SP8. P-wave record sections are reduced by a velocity of 6 km/s, the positive offset corresponds to the north direction while the negative represents the south direction (inset is the corresponding one dimensional (1D) seismic velocity-depth function).

(Fig. 2). However, late Permian basaltic rocks present in this area, may be distal members of the Emeishan continental flood basalts (Enkelmann et al., 2007; Song et al., 2004).

3. Seismic data and phase analysis

3.1. Layout and observations

The Simao-Zhongdian DSS profile is 600 km in length and starts near Simao city in the south, extends northward through the Langcangjiang fault (LCJF), Red River fault (RRF) and Lijiang-Ninglang fault (LNF) (Fig. 2), and terminates to the north at Zhongdian city. The Simao-Zhongdian profile is the main profile of the "Dian-Shen 8687" project. Eight shots were fired along the profile at an interval of about 40–140 km. The explosive charge of each shot varied from 1500 kg to 3000 kg. One of the shots (SP3) was an underwater explosion and others were multi-borehole explosions. The depth of the borehole explosions were emplaced in 17–25 m deep boreholes. Along the profile, 447 mobile seismographs were deployed with an interval of about 1–3 km. The experiment data was acquired by eight institutes from China Earthquake Administration from April to June 1987. The data has a very high signal-to-noise ratio due to relatively low industrialization and sparse freeways in the 1980s.

3.2. Seismic phases on the record sections

Figs. 3 and 4 show the seismic record sections of SP1, SP8 and SP4, with time reduced by distance divided by 6 km/s. On the record sections, Pg is the head wave or diving wave propagating in the crystalline basement and is a clear phase that contains detailed information from the sediment and the upper crust. PmP is the reflected wave from the crust-mantle boundary and has strong amplitude. It usually appears at 80–120 km from the shot point and can be observed as far as 300 km (Figs. 3c, 4c). Pn is refracted within the uppermost mantle and becomes the first arrival at a distance greater than 170 km and 200 km (Figs. 3a, c, 4a, c). All three phases can be traced in all shots in our profile and arrival times of these phases can be picked with high accuracy. In addition, one or two reflected phases, called P_1P and P_2P, from intra-crustal interfaces, can be identified on individual record sections. These two phases are distinctly weaker than PmP, which indicates that the intra-crustal interfaces have a lower P-wave impedance contrast.

In the southern record section of our profile (Figs. 3a, 4a), the first Pg arrivals can be traced at a distance up to 100 km at a reduced time of about 0.5–1.0 s. PmP arrivals are clear at 90–100 km and can be traced to 200–250 km. The amplitude of Pn is strong and this phase can be traced to 260 km, which may indicate a relatively high velocity gradient in the uppermost mantle (Braile and Smith, 1975). Only one group of intra-crust reflection P_1P can be recognized, whose travel times are obviously delayed with respect to the Pg phase. This indicates that velocity of the upper crust is relatively low.

For the northern record section of the profile (Figs. 3c, 4c), Pg arrivals can be traced up to a distance of 120 km and the travel times vary drastically, indicating a heterogeneous upper crustal structure. Pg phases from the north end section of the profile (Fig. 3c) show much earlier travel times than other sections, indicating a high velocity in the upper crust. PmP arrivals are quite late, with a reduced time of about 4 s at 150 km (Fig. 3c), and are 2 s later than the SP1 record section (Fig. 3a) for the same distance. This indicates a greater crustal thickness in the northern section of the profile. Pn shows relatively weaker amplitude in the northern section than the southern section, with an apparent velocity of about 7.9–8.0 km/s. Two groups of intra-crust reflection P_1P and P_2P can be recognized (Figs. 3c, 4c), indicating the crystalline crust is divided into three layers.

4. Modeling methods

A more accurate upper crustal velocity model can be constrained by first arrivals of Pg, which always have the highest signal to noise ratio, and also can reduce the uncertainty of the velocity in middle-lower crust. So the 2D finite-difference inversion method (Vidale, 1988, 1990; Hole, 1992) was used to determine the upper crustal structure in our paper. The inversion is based on the eikonal equation and the plane-wave approximation. The grid nodes in our model have an equal horizontal and vertical spacing of 0.5 km. Travel times in every grid cell can be calculated from the mean slowness of each grid by using the finite-difference operator. This method is much faster than the two-point ray tracing method and avoids the failure of the ray tracing in highly heterogeneous media. A back-projection algorithm is used in the inversion process, and the travel time perturbations of the slowness can be added to the model during the iterations. The computational speed of this scheme is related to the number of the grid nodes, but is not affected by the complexity of the model. Therefore, this method is very suitable for the modeling of heterogeneous upper crustal structure. The spatial resolution of the resultant seismic velocity model can be estimated by the number of rays in each grid node (Fig. 5) and regions without ray coverage should be ignored.

The 2D ray tracing method was used to model the structure of the crust and uppermost mantle (Cerveny et al., 1977; Cerveny and Psencik, 1984). Even if this method is used more than 30 years, it is still a robust ray tracing method helping us to discover the deep earth (Grad et al., 2003; Wang et al., 2007; Wang et al., 2013). All of the recognizable seismic phases (Pg, P_1P, P_2P, PmP and Pn) mentioned above were used to determine the final model. First, the initial model was constrained by using the $x^2 - t^2$ method, 1D travel time fitting method and the 1D reflectivity method (Giese et al., 1976; Fuchs and Muller, 1971; Braile and Smith, 1975). The average crustal velocity above a reflector and the depth of each interface can be calculated from the reflected waves. The velocity contrast at an interface can be estimated from the amplitude information using the reflectivity method (Fuchs and Muller, 1971). Repeated modification of the crust-mantle velocity model was needed to obtain an optimal fitting between the theoretical and observed travel times. The 1D velocity model for each shot can then be obtained (Fig. 3 and Fig. 4). The 1D initial models were used to create an initial, laterally-varying 2D model and, using the trial and error method, the travel times were iteratively recalculated many times until the data misfits were reduced to a level of 0.1 s. The final 2D crustal model is

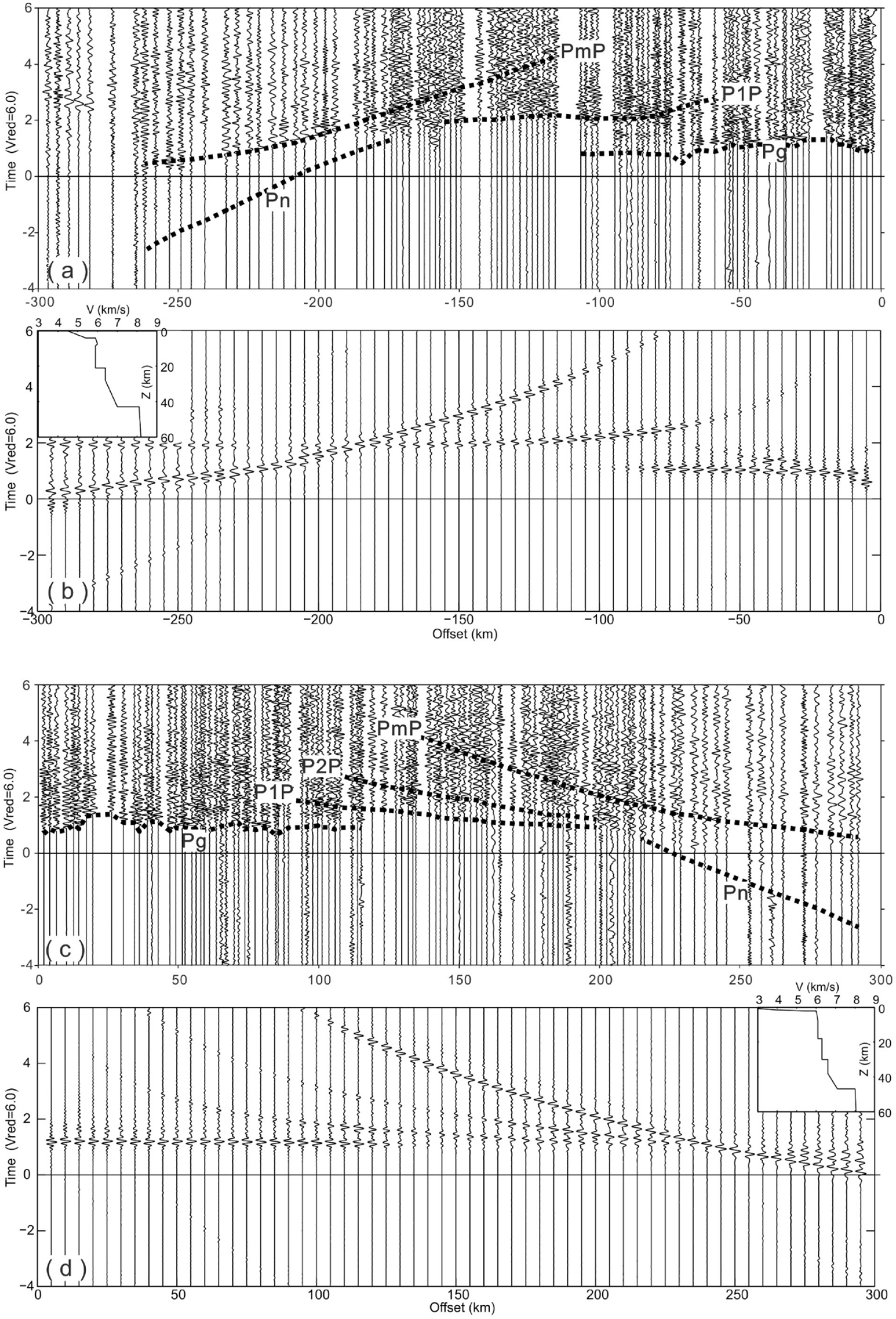

(caption on next page)

Fig. 4. P-wave record sections and associated synthetic seismograms. (a) South branch record section of SP4. (b) South branch synthetic seismogram record section of SP4 (Inset is the corresponding one dimensional (1D) seismic velocity-depth function). (c) North branch record section of SP4. (d) North branch synthetic seismogram of SP4 (inset is the corresponding one dimensional (1D) seismic velocity-depth function).

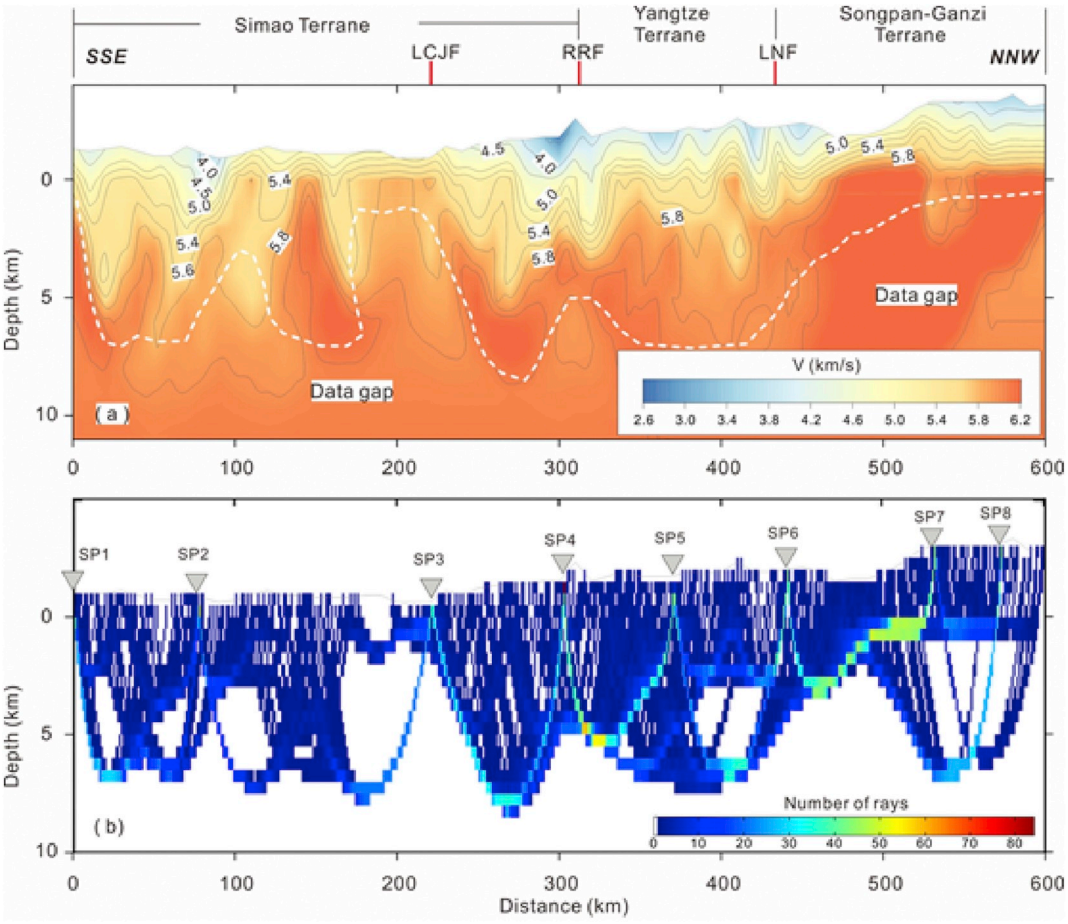

Fig. 5. (a) Two-dimensional velocity structure of the upper crust along the Simao-Zhongdian DSS profile derived from finite difference travel time inversion of Pg arrivals. Names of the depicted faults are: LCJF-Lancangjiang fault; LNF- Lijiang-Ninglang fault; RRF-Red river fault. The white dashed line shows the boundary of ray coverage. (b) The distribution of ray density. Inverted red triangles represent shot points. (For interpretation of the references to color in this figure legend, the reader is referred to the web version of this article.)

presented in Fig. 6. Adjustments to the 2D model followed the principle of moving iteratively from shallow to deep levels in the model (Fig. 7).

Uncertainties of the final 2D velocity model mainly depend on the correct identification of the seismic phases, the density of the rays, the shot point interval, and the receiver spacing (Liu et al., 2006). We made an uncertainty test about the Moho depth (Fig. 8). Maintaining the velocity invariable, the uncertainty of the Moho depth is about ± 1 km– ± 2 km. If the PmP phase is clear in the offset of 50–150 km, the Moho uncertainty is less than ± 1 km or even ± 0.5 km. The uncertainty of the velocity is about ± 0.1 km/s in a relatively simple crustal structure and ± 0.2 km/s for a complicated crustal model (Grad et al., 2003; Jia et al., 2014b). We also made a comparison of Pg travel times and upper crustal velocity in SP8 and SP1 record section, which revealed that the north part of our DSS profile has a relatively higher upper crustal velocity than the south part, and the difference value is 0.3 km/s (Fig. 9).

5. Velocity models of crust and uppermost mantle

5.1. Upper crustal velocity structures

A total of 528 travel times of first arrivals, collected from 8 shots on the Simao-Zhongdian DSS profile were used to invert the upper crustal velocity. Upper crust model was parameterized by 37,231 square cells with 0.5 km length. There were 1201 square cells in the horizontal direction and 31 in the vertical direction. The final model (Fig. 5) was obtained after 20 iterations, and the root-mean-square (RMS) travel time residual was reduced from 0.63 s to 0.10 s.

The velocity structure in the upper crust is quite heterogeneous, and shows unique characteristics within each tectonic unit. If we use the contour line of 5.8 km/s as the crystalline basement, the Simao terrane has relatively thin sediments (1–2 km) in the middle section and very thick sediments (4–5 km) in the north and south parts. In western

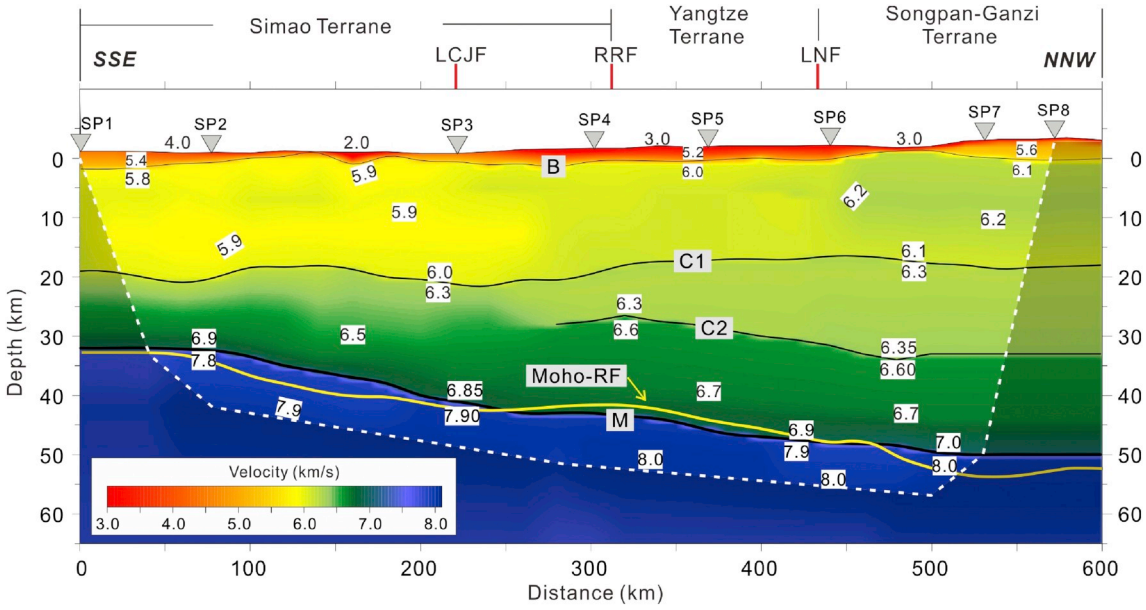

Fig. 6. Two-dimensional crustal P-wave velocity model along the Simao-Zhongdian profile from the Simao terrane in the south to the Songpan-Ganzi terrane in the north. The top panel shows the tectonic units and faults which are crossed by the profile: LCJF-Lancangjiang fault; LNF-Lijiang-Ninglang fault; RRF-Red River fault. Red inverted triangles indicate shot point locations. The top of the crystalline crust is indicated by "B" and the crust-mantle boundary by "M". C1 and C2 are interfaces within the crystalline crust. The yellow line named "Moho-RF" is Moho interface based on the receiver function results (Wang et al., 2017).

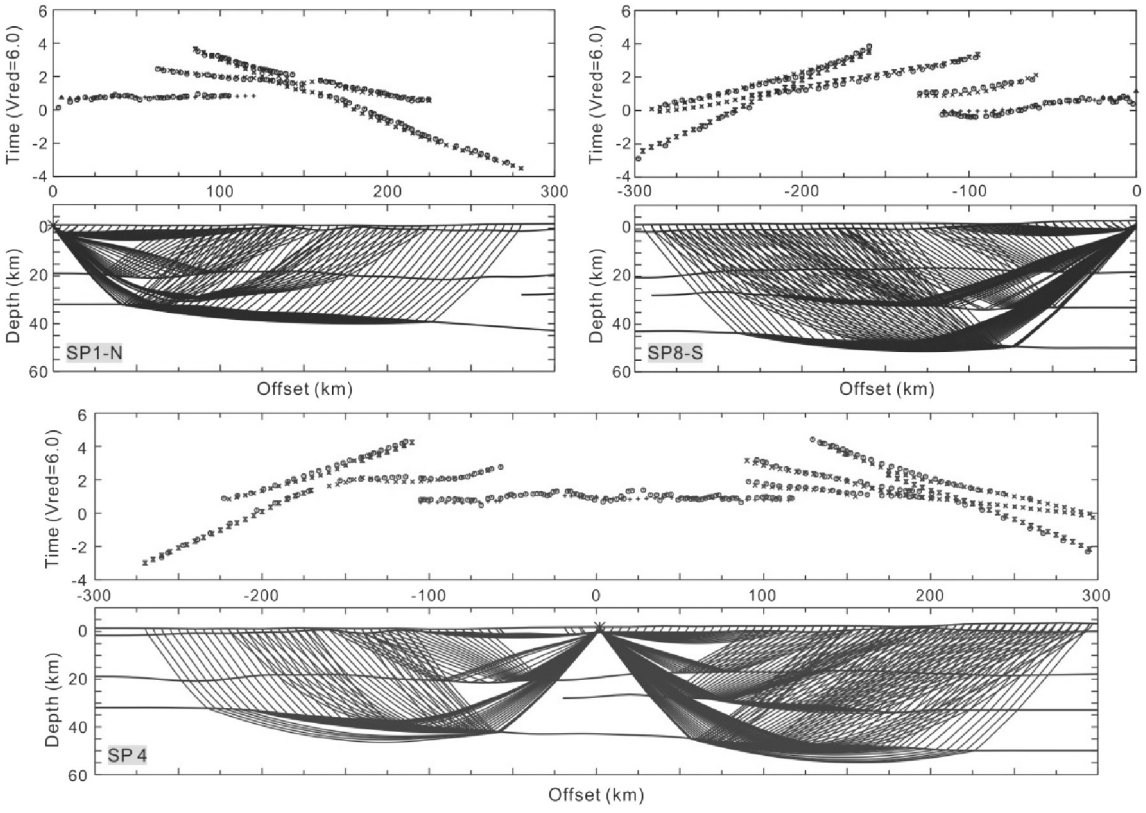

Fig. 7. Ray tracing and travel time fitting diagrams of SP1, SP8 and SP4. Small circles in the top panels show the measured travel times, while other symbols show the calculated travel times. The positive offset represents the north direction and negative represents the south.

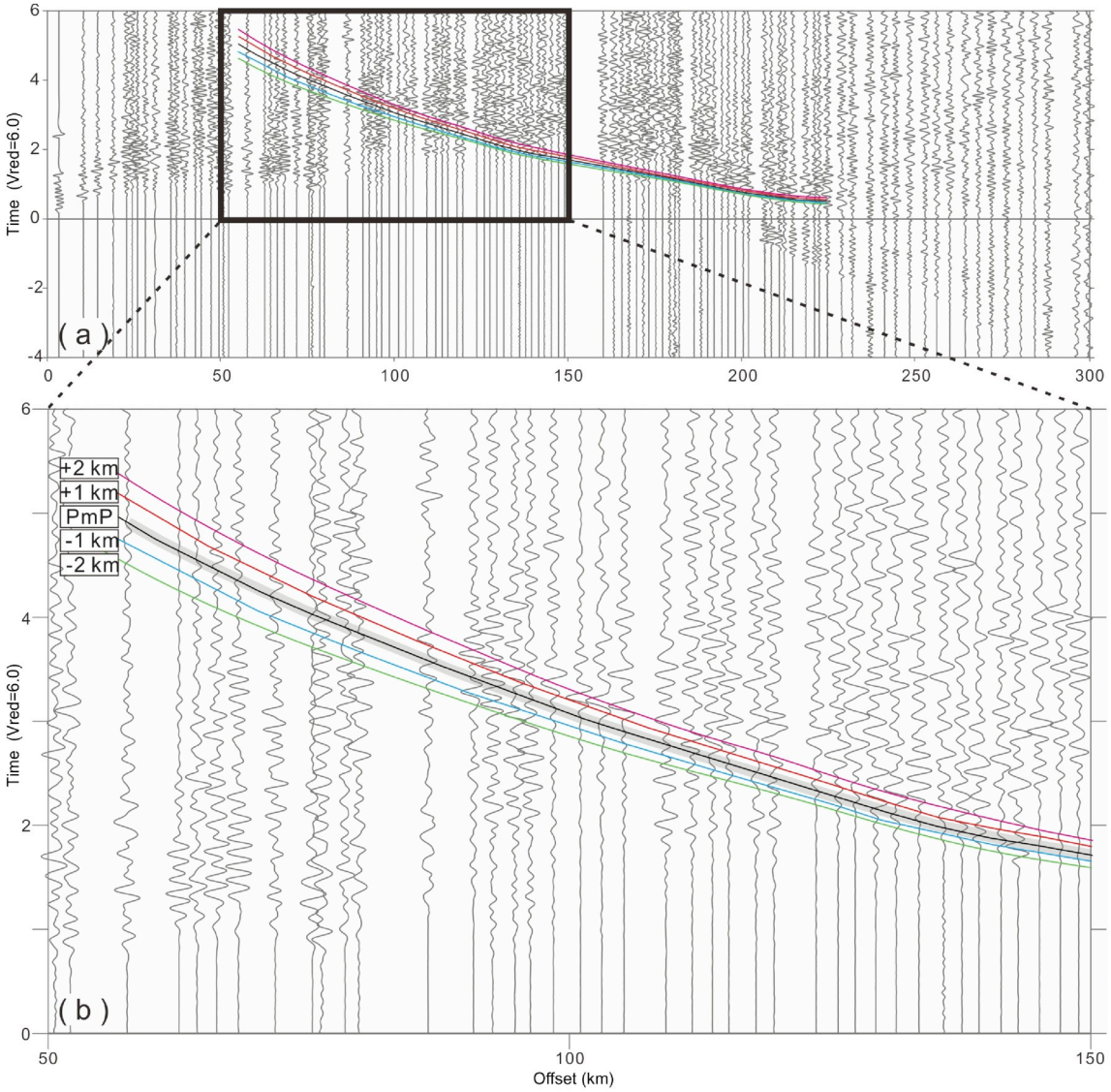

Fig. 8. (a) Resolution test of PmP arrival times for Shot point 1 (SP1). The arrival times of PmP phase reflected from Moho in the final model are shown by a dark line, and the arrival times with the depth perturbed by ± 1 km and ± 2 km are shown by color lines. The grey belt extends across the uncertainty interval of ± 0.1 s around the arrival times. (b) Inset shows zoomed parts of sections between offset 50 and 150 km.

Yangtze terrane (WYZT), the thickness of the sediments is 4–5 km and the velocity is relatively low on the surface due to some Cenozoic sedimentations. The isolines of the velocity vary within the terrane strongly in the horizontal direction, which is likely a result of some deformation that has occurred between different terranes. In the north section of our DSS profile, sedimentary cover thickens from 2 km in the south part to 4 km in the north. High velocity (6.2 km/s) materials exist beneath the sediment in the Songpan-Ganzi terrane. A large variation in velocity occurs beneath the fault zones, such as the LCJF, RRF and LNF, which may absorb a significant amount of the tectonic deformation.

5.2. Crustal and uppermost mantle velocity structures

The modeling results (Fig. 6) revealed lateral variations of P-wave velocity in the crust and uppermost mantle, as well as significant variations in the Moho depth. The crustal thickness increases gradually from 34 km beneath the Simao terrane in the south to about 53 km beneath the Songpan-Ganzi terrane in the north.

In the southern part of our profile (Simao terrane), the Moho depth deepens from 34 km in the south to 45 km beneath the RRF. The average crustal thickness and the average crustal velocity are 38.2 km and 6.10 km/s, respectively. Only one group of reflected interfaces can be measured in the crystalline crust, with a depth of about 20 km. The seismic amplitude information (Fig. 3 and Fig. 4) is matched by a model with 6.0 km/s and 6.3 km/s above and below the C1 interface. The upper crustal velocity is about 5.9 km/s at the depth of 5–15 km, relatively lower than surrounding area, and the horizontal extent is about 200 km. There are no obvious reflected phases that can be identified between the P_1P and P_mP phases (Fig. 3 and Fig. 4), which indicates that the C2 interface cannot be measured in the Simao terrane. The

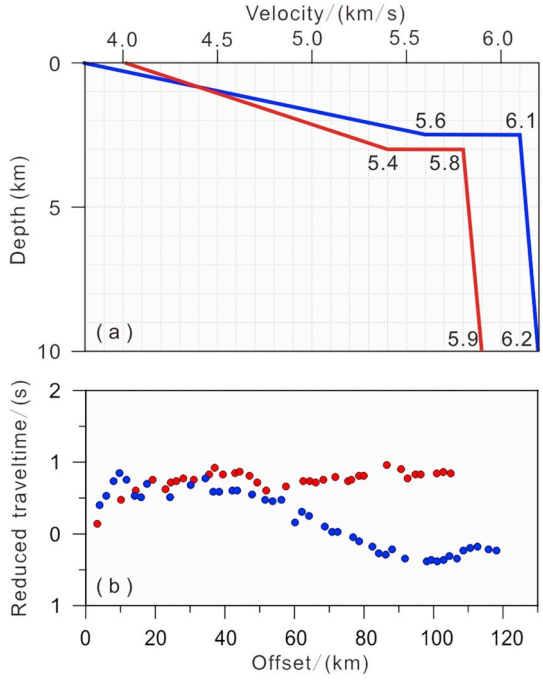

Fig. 9. Upper crustal P wave velocity and Pg travel time picks in the south and north of Simao-Zhongdian profile. (a) Upper crustal P wave velocity. Red line is derived from SP1 (Fig. 3a) and Blue line is derived from SP8 (Fig. 3c). (b) Pg travel time picks for SP1 (red dots) and SP8 (blue dots). Reduced velocity is 6.0 km/s. (For interpretation of the references to color in this figure legend, the reader is referred to the web version of this article.)

velocity above the Moho is 6.85–6.90 km/s and 7.8–7.9 km/s in the uppermost mantle.

The Yangtze terrane, in the middle of the profile, has a crustal thickness of 48 km and a whole-crustal average velocity of 6.16 km/s. Two of intra-crustal interfaces were detected at depths of about 20 km and 30 km. The seismic velocity increases gradually from 6.0 km/s below interface B to 6.1 km/s above interface C1. Velocities between interface C1 and C2 reveal a low velocity gradient feature in this layer, while velocities between interface C2 and the Moho show a relatively high velocity gradient, from 6.6 km/s to 6.9 km/s in a layer thickness of about 15 km. The velocity of the uppermost mantle is 7.9–8.0 km/s, slightly higher than the south of RRF.

The north section of the Simao-Zhongdian DSS profile extends into the Songpan-Ganzi terrane for a distance of about 150 km. The average Moho depth is 52 km and crustal average velocity is 6.32 km/s, which is 9–37% deeper and 2–4% higher velocity than the other two tectonic units. The sedimentary cover is much thinner between Shot Point 6 (SP6) and SP7, which agrees with the results from the finite difference method (Fig. 5). Intra-crustal interfaces are similar to the Yangtze terrane, but the C2 interface is slightly deeper. The upper crust velocity is about 6.2 km/s at a depth of 5–15 km, which increases the crustal average velocity. The velocity of the uppermost mantle is relatively high (8.0 km/s).

6. Discussion

6.1. Comparison with other DSS profiles' results

We chose four high-quality DSS profiles (Fig. 10a), which were acquired during the period 2009–2015, to compare the crustal structure of different tectonic units in our study area. This study area is divided into three major tectonic domains: the Indochina block, Yangtze craton and Tibetan Plateau. We calculated the average thickness and average velocity in each layer for these crustal models. The crust was sub-divided into four layers, sediments (V_p < 5.7 km/s), upper crust (5.7 < V_p < 6.4 km/s), middle crust (6.4 < V_p < 6.8 km/s) and lower crust (6.8 < Vp < 7.3 km/s), according to the high-pressure laboratory measurements for felsic, intermediate and mafic rock types (Christensen and Mooney, 1995). Considering the high heat flow in this region, 72–82 mW/m^2 (Hu et al., 2000; Wang, 2001), the compressional wave velocities will decrease about 0.05–0.2 km/s for the same lithology in a relatively high temperature (Christensen and Mooney, 1995, Table 4). Therefore we modified the criterion to be: sediments (V_p < 5.7 km/s), upper crust (5.7 < V_p < 6.3 km/s), middle crust (6.3 < V_p < 6.7 km/s) and lower crust (6.7 < Vp < 7.2 km/s). The velocity columns in Fig. 10b were arranged by numbers with round brackets, according to the tectonic units they transected.

The Indochina block has a similar crustal structure within different sub-terranes. Velocities in the upper, middle and lower crust are 5.9–6.0 km/s, 6.4–6.5 km/s and 6.8 km/s. Columns 1 and 2 in Fig. 10b intersect each other (Fig. 10a) and have almost the same velocities and interfaces depth in the intersection (Fig. 11). Crust thickens from 32 km beneath Simao to 42 km beneath RRF and 37–39 km beneath Baoshan terrane (BST) and Tengchong terrane (TCT). In addition, the Simao terrane (SMT) and TCT reveal relatively lower crustal velocities than the BST, suggesting that they may experience different tectonic processes. Volcanic activities in the TCT and more felsic composition in the SMT may be responsible for this relatively low velocity crustal structure (Deng et al., 2014a, 2014b; Lei et al., 2009). The lower crust is very thin and almost does not exist in the Indochina block, suggesting only a small volume or almost missing the mafic rocks in this block.

Velocity columns show distinct differences within the western Yangtze terrane (WYZT). All four columns (columns 5–8 in Fig. 10b) are located to the west of the Xiaojiang fault, which is considered to be an important fault in southwest China. It is likely to cut through the whole crust (Wang et al., 2009; Xu et al., 2015). Moho depth increases from 40 km in the south (columns 5 and 6 in Fig. 10b) to about 50 km in the west and north of the WYZT (columns 7 and 8 in Fig. 10b). Thicknesses of each layer inside the crystalline crust varies greatly from 16 to 21 km in the upper crust, 5–21 km in the middle crust and 2–10 km in the lower crust. Lower crustal thicknesses in columns 6 and 8 are distinctly larger than columns 5 and 7 in Fig. 10b, and velocities in columns 6 and 8 are relatively higher than columns 5 and 7. Xu et al. (2015) argued that the inner zone of the Emeishan large igneous province (LIP) has a high velocity crustal structure (column 8 in Fig. 10b) due to volcanism during the late Permian period and possible crustal intrusions, which may be a result of a mantle plume. Our comparisons demonstrate that the inner zone of the WYZT experienced higher levels of magmatism than the marginal areas.

The Songpan-Ganzi terrane (SGT) has the thickest crust in this region, about 52 km. Upper crustal thickness is 19 km, with an average velocity of about 6.15 km/s, which resembles the northern part of the WYZT (column 8 in Fig. 10b). The middle and lower crust present similar characteristics as the west WYZT (column 7 in Fig. 10b). Proterozoic rocks, Permian basaltic rocks and Triassic deposits are all distributed in the SGT, which reflects the active tectonics of this area (Enkelmann et al., 2007; Song et al., 2004). High velocity upper crust beneath SGT may indicate that the basalts derived from Emeishan magmatism are overlain by Permian marble and slate, and then overlain by Triassic clastic rocks (Song et al., 2004).

To the north of our profiles (lines 10–12 in Fig. 12e), three previous

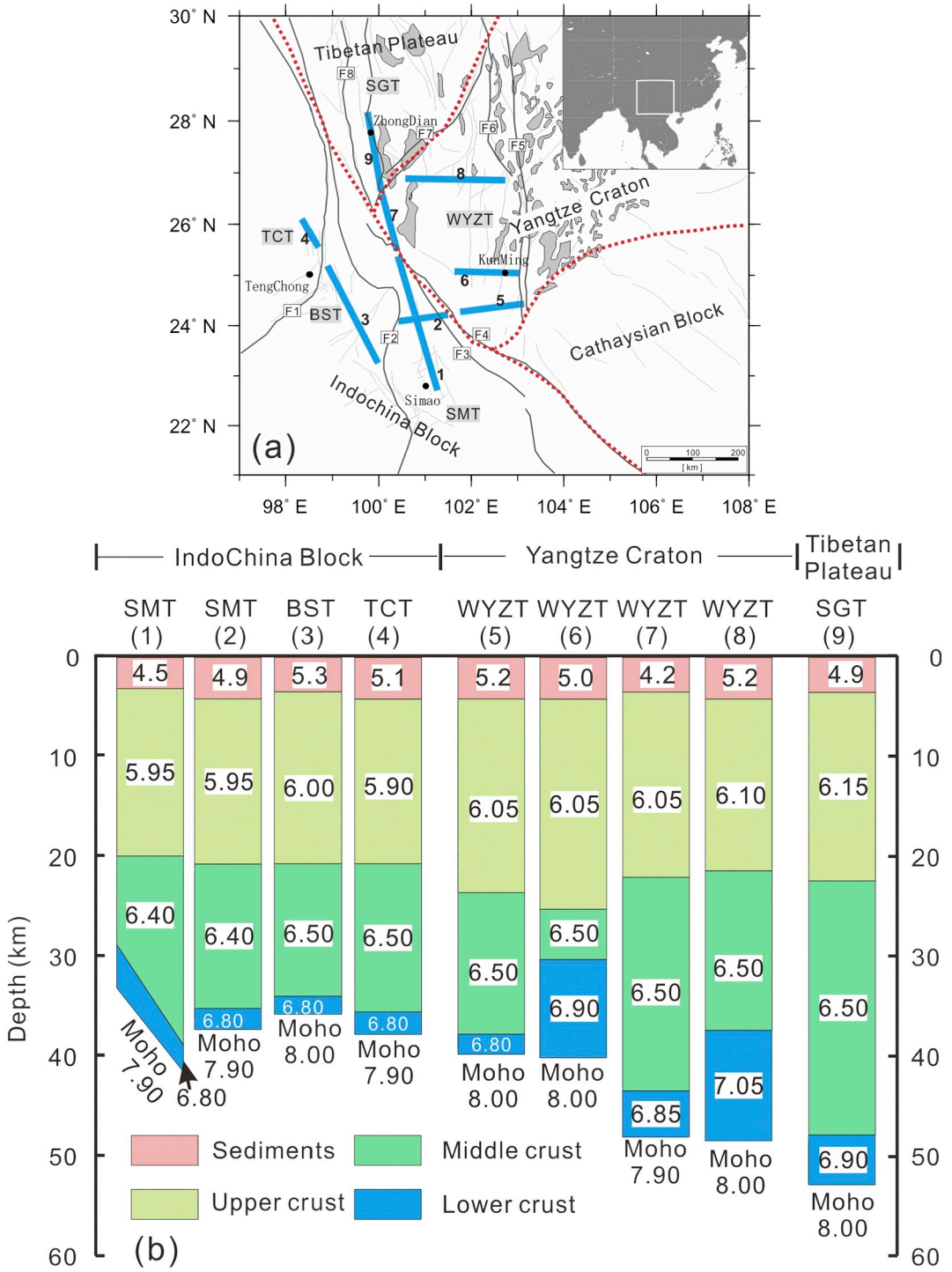

Fig. 10. (a) Location map of the representative DSS sections. Blue lines indicate the sections we compared with each other and the numbers beside them are corresponding to the numbers with round brackets in (b). Grey shaded regions indicate the distribution of Emeishan flood basalts. The names of geological units are as follow: TCT: Tengchong terrane; BST: Baoshan terrane; SMT: Simao terrane; WYZT: Western Yangtze terrane; SGT: Songpan-Ganzi terrane. (b) Representative seismic velocity-depth functions for P-wave in the study area. The top panel shows the tectonic units. (For interpretation of the references to color in this figure legend, the reader is referred to the web version of this article.)

DSS profiles provide us with an opportunity to compare the crustal structure and the relation to tectonics in a more extensive region. On our line and line 10 ((a) and (b) in Fig. 12), the Moho deepens from 30 km in the south to 60 km in the middle, and then decreases to 50 km at the north end. The thickness of the crust decreases from nearly 60 km in the west to about 40 km in the east ((c) and (d) in Fig. 12). The crustal velocity beneath Yangtze terrane (YZT) reveals much higher than Songpan-Ganzi terrane (SGT), which exhibits a rigid cratonic

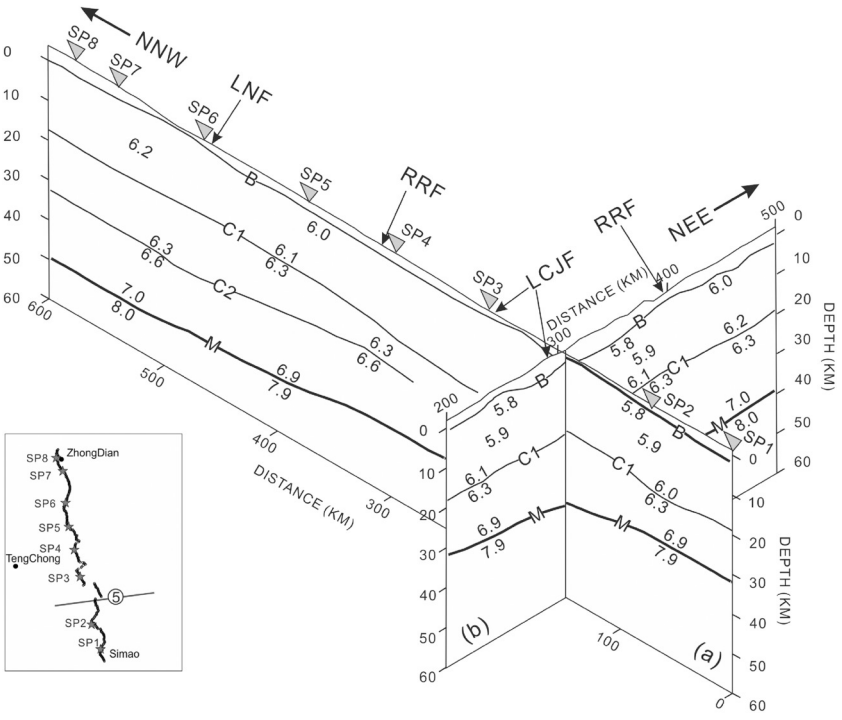

Fig. 11. Interpreted crustal cross sections for our line (a) and line 5 (b) in Fig. 1. Major faults, velocities, and main crustal boundaries are indicated. The names of faults are as follow: LCJF-Lancangjiang fault; LNF-Lijiang-Ninglang fault; RRF-Red River fault. The grey inverted triangles represent shot point locations. The top of the crystalline crust is indicated by "B", and the crust-mantle boundary by "M". C1 and C2 are interfaces within the crystalline crust. Inset map shows the location of the DSS lines.

structure in the east and a relatively plastic structure northwest of Longmenshan fault (LMSF).

We also compare our result with those of Lin et al. (1993) and Zhang et al. (2009) for the same profile (Fig. 13). These three studies share the same characteristics of the Moho, deepening from the south to the north, although Lin et al.'s (1993) Moho depth is 1–2 km deeper than ours and that of Zhang et al. (2009). Velocities inside the crust show the same pattern in the upper crust, being relatively lower beneath Simao terrane (SMT) and higher beneath Songpan-Ganzi terrane (SGT), although there are some discrepancies in the lower crust. Interfaces within the crust are quite different for these three studies due to differences in the identification of reflected phase. The main differences are that we did not recognize the interface at the depth of 15 km along the whole profile, nor the interface at the depth of 25 km beneath SMT. The results of Zhang et al. (2009) show that the interfaces inside the crust are discontinuous features beneath SMT, which is due to the fact that the reflected phases are not always clear. We also collected earthquakes that occurred during the 11 year time period 2008.01–2018.01, with a magnitude larger than 3.0, and project these events on the Simao-Zhongdian profile at a distance less than 40 km (Fig. 13a). The seismic events mainly occur in the south within the Simao and Yangtze terranes above interface C1. This indicates that interface C1 marks the transition from brittle to ductile materials, and the ductile layer thins from north to south.

6.2. Comparison with other seismological results

Passive seismological tomography can provide constrains for crustal thickness, S wave velocity, Poisson's ratio, anisotropy and seismic wave attenuation (Chen et al., 2013; Zhao et al., 2013; Sun et al., 2014; Wang et al., 2014b; Fu et al., 2017; Li et al., 2017; Wang et al., 2017). The crustal thickness derived from receiver function method reveals that the crustal thickness in the margin of SE Tibet shallows from 60 to 65 km beneath the northeast part to the east, the southeast, and the south direction, with the value of about 30–35 km (Bai et al., 2010b; Chen et al., 2010; Wang et al., 2017; Yu et al., 2017; Zhang et al., 2017). These results show the same pattern with our results from DSS method. We also transected the receiver function results (Wang et al., 2017) along our profile, where the Moho depth based on receiver function method (Moho-RF) shows the same trend with "M" (Fig. 6). The differences of these two Moho depths in localized region may be caused by the distribution of the broadband seismographs. S wave velocity reveals relatively lower in SE margin of Tibet, according to joint inversion of receiver functions and Rayleigh wave dispersion, especially beneath Songpan-Ganzi terrane (SGT), western Yangtze terrane (WYZT) and Tengchong terrane (TCT). From the P wave velocity columns (Fig. 10b), we only observe the upper crustal velocity is relatively lower beneath TCT and SMT, and the lower crust is very thin beneath this region, except beneath WYZT. By comparing these results, the S wave velocity in the crust decreases significantly, while the P wave velocity does not. Consequently, the Poisson's ratio increases to 0.26–0.28 beneath WYZT, or even higher than 0.28 beneath SGT, 0.32 beneath TCT, which may indicate more mafic compositions or even partial melting (Wang et al., 2017). Seismic anisotropy from shear wave splitting evidence demonstrates the deformation within the crust and upper mantle are decoupled in this region, and the fast polarization directions for Pms are approximate along NW-SE, which may indicate the direction of lower crustal flow (Chen et al., 2013). High seismic wave attenuation (Q_{Lg} = 200) in this region also indicate high temperatures and even partial melting, which may decrease the viscosity of the rocks and cause flow (Zhao et al., 2013).

6.3. Crustal composition

Crustal composition can be constrained by making comparisons with laboratory measurements of seismic velocity for a wide range of

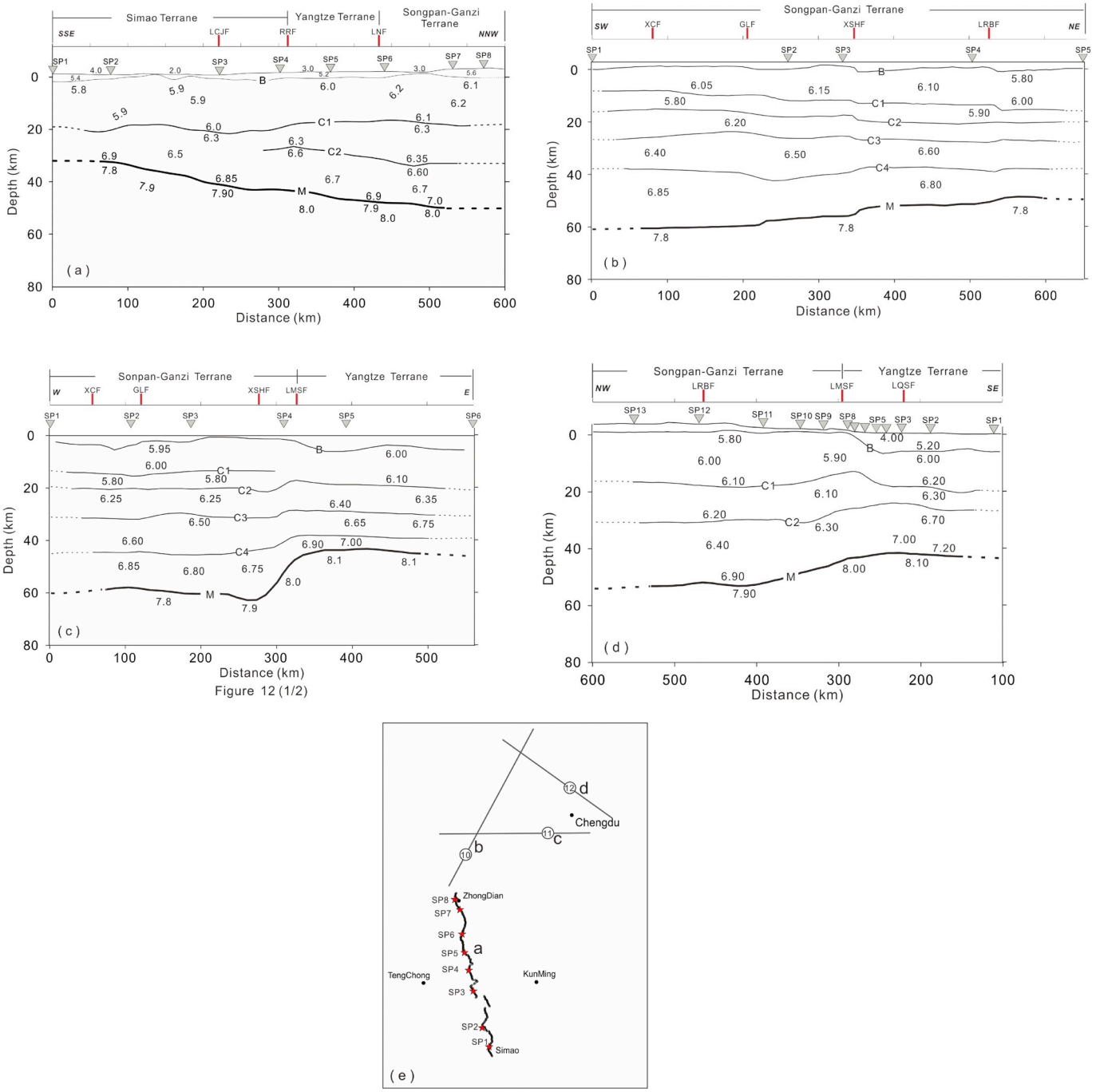

Figure 12 (1/2)

Fig. 12. Comparison of the crustal structure along profiles: (a) This study; (b) Benzilan-Tangke (Line 10 in Fig. 1) [Wang et al., 2007]; (c) Zhubalong-Zizhong (Line 11 in Fig. 1) [Wang et al., 2007]; (d) Suining-Aba profile (Line 12 in Fig. 1) [Jia et al., 2014a]. (e) The location of DSS lines. The top panel shows the tectonic units and faults which are crossed by the profile: GLF-Ganzi-Litang fault; LCJF-Lancangjiang fault; LMSF-Longmenshan fault; LNF-Lijiang-Ninglang fault; LQSF-Longquanshan fault; LRBF-Longriba fault; RRF-Red River fault; XCF-Xiangcheng fault; XSHF-Xianshuihe fault. Grey inverted triangles indicate shot point locations. The top of the crystalline crust is indicated by "B" and the crust-mantle boundary by "M". C1, C2, C3 and C4 are interfaces within the crystalline crust.

rocks that are found in the crust (Christensen and Mooney, 1995). The P-wave seismic velocity intervals that correspond to the crustal composition are: sedimentary and basement rocks (V_p < 5.7 km/s), felsic rocks (5.7 < V_p < 6.3 km/s), intermediate rocks (6.3 < V_p < 6.7 km/s) and mafic rocks (6.7 < Vp < 7.3 km/s). Based on this reference, we acquired the crustal composition along the Simao-Zhongdian DSS profile (Fig. 14). The whole profile is characterized by a thick upper and middle crust and very thin lower crust, which indicates that a significant proportion of the crust consists of felsic materials, while just a small percentage of mafic rocks in the lower crust.

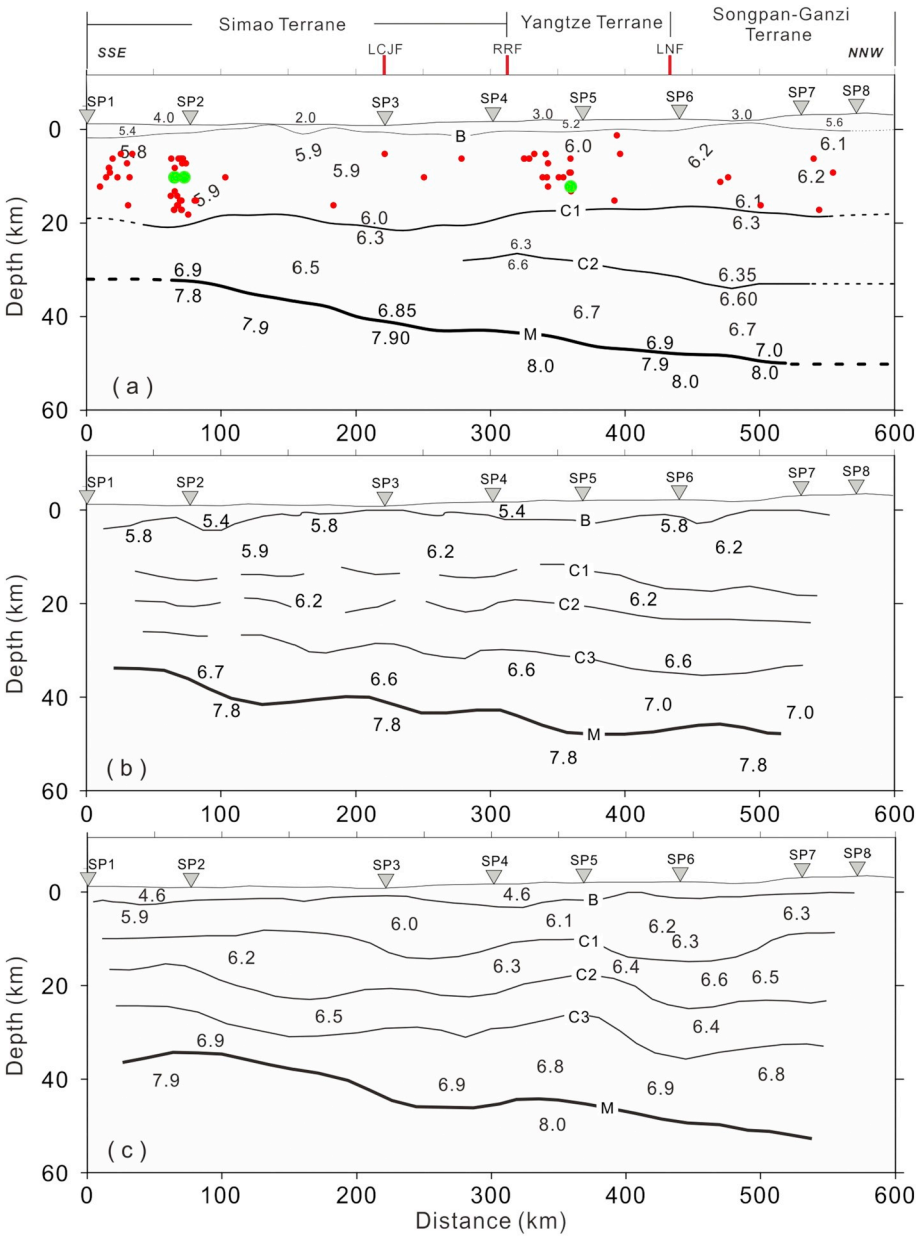

Fig. 13. Comparison of the crustal velocity structure along the Simao-Zhongdian profile: (a) This study. The dots represent the distribution of seismic events occurred during the period of 2008.01–2018.01 less than 40 km from the Simao-Zhongdian profile. The red dots show a magnitude of 3.0–5.0 and the green dots represent a magnitude of 5.0–7.0; (b) (Zhang et al., 2009); (c) (Lin et al., 1993). The top panel shows the tectonic units and faults that are crossed by the profile: LCJF-Lancangjiang fault; LNF-Lijiang-Ninglang fault; RRF-Red River fault. Grey inverted triangles indicate shot point locations. The top of the crystalline crust is indicated by "B" and the crust-mantle boundary by "M". C1, C2 and C3 are interfaces within the crystalline crust. (For interpretation of the references to color in this figure legend, the reader is referred to the web version of this article.)

The Simao terrane (SMT) exhibits a relatively low P-wave velocity layer (5.9 km/s) in the upper crust (Fig. 6). This layer is inferred to be rich in silicic rocks, which may have resulted from granitic intrusions during the collision of the Simao terrane, Baoshan terrane and Yangtze craton in the late Variscan-Indosinian stage (Deng et al., 2014a, 2014b; Ma, 2002). By comparison, a relatively high velocity layer (6.2 km/s) exists beneath the Songpan-Ganzi terrane (SGT). We infer that these higher velocity rocks may be due to the presence of some basaltic rocks, which were affected by the Emeishan LIP. The lower crust along the profile is a thin layer and almost disappears in some regions. The high heat flow of 72–82 mW/m^2 (Hu et al., 2000; Wang, 2001) in this region could indicate high temperatures in the lower crust. Lithospheric delamination and asthenospheric upwelling are considered to be processes that have reduced the thickness of the lithosphere in the North China Craton (Gao et al., 2002). Geochemical evidence show the Songpan-Ganzi terrane's lithosphere was delaminated after Triassic period due to the collision of Songpan Ganzi terrane and Yangtze block (Zhang et al., 2007). Likewise, delamination may have reduced the thickness of the lower crust in our study area (Zhai et al., 2007).

6.4. Tectonic activity

Accompanied by the closure of the Paleo-Tethys Ocean in the Permo-Triassic (290–205 Ma), Gondwana-derived micro-continental blocks and arc terranes coalesced and formed what is now called

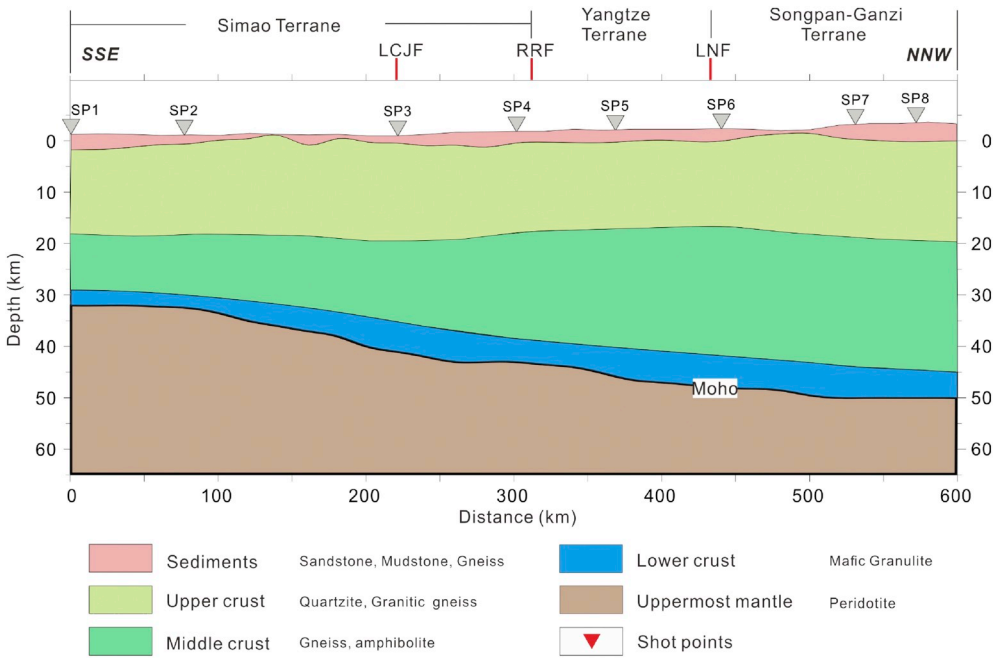

Fig. 14. Geologic cross section along the Simao-Zhongdian profile derived from the P-wave velocity model (Fig. 6). The top panel and the name of faults are the same as in Fig. 6.

South China continent. Two sub-parallel ophiolite complexes are distributed along the Lancangjiang fault, Jinshajiang fault and Red River fault, which are considered to be suture zones (Fig. 2). In addition, Emeishan flood basalts and their intrusive equivalents, triggered by rifting or mantle plume eruption in the latest Permian (250 Ma), changing the crust significantly, and increasing the average P wave velocities in the crust (Xu et al., 2001; He et al., 2003; Xu et al., 2015).

Since Cenozoic period, the continental collision between India and Eurasia result the thickening of the crust and uplift of the Tibetan Plateau, and make great changes to the margin of Tibet. In our study area, many geological and geophysical observations provided various types of evidence to support the lower crustal flow model (Royden et al., 1997; Clark and Royden, 2000; Enkelmann et al., 2006; Wang et al., 2007; Royden et al., 2008; Bai et al., 2010a; Zhao et al., 2013; Liu et al., 2014). High electrical conductivity, high heat flow, low S wave velocity and high Poisson's ratio in SE Tibet suggest that the weak and ductile material exists in the lower crust. Crustal thickness in SE Tibet, constrained by DSS and receiver function results (Wang et al., 2010), is about 60 km in Songpan-Ganzi terrane and is 42 km beneath Yangtze craton in the east, with a gradient belt beneath Longmenshan (LMS) Mountain, and reaches 34 km beneath Simao terrane in the southern direction with a relatively smooth variation (Figs. 12, 15). According to the distributions of earthquakes along the DSS profiles (Fig. 15), the ductile layers (the areas without earthquakes) thins from the north to the south, and from the west to the east, may indicate the ongoing deformation in the middle-lower crust. Synthesizing all geophysical and geological results, we infer that this variation of Moho depth and ductile layers are due to viscous crustal flow from the Tibetan plateau to the Indochina block in the south, whereas flow is stopped when encountering the rigid Yangtze craton along the LMS Mountain. Similarly, apatite fission-track thermochronology data demonstrate that the crustal materials flow to the north of Yangtze craton, which belongs to western Qinling Mountain, resulting a smooth Moho as well (Enkelmann et al., 2006; Wang et al., 2010). Meanwhile, seismic anisotropy observations demonstrate the deformation with the crust and upper mantle are decoupled in SE margin of Tibet, which consistent with the canonical crustal flow model according to Royden's argument (Royden et al., 1997; Chen et al., 2013). High attenuation evidence from Lg-wave Q tomography also shows two channel flows exist in this region (Zhao et al., 2013).

7. Conclusions

In this paper, together with available geological and geophysical constraints, we made some comparisons with the crustal P wave velocity, S wave velocity, Poisson's ratio, seismic anisotropy and attenuations in the SE margin of Tibetan Plateau. We identified the different characteristics of crustal structure in each geologic terrane. The upper crust presents a relatively lower velocity in the Indochina Block and much higher velocity in the SGT and northern WYZT, which may related to the collision process and Emeishan LIP. The lower crust is thinned distinctly beneath the Indochina Block and the surrounding area of the WYZT, which we speculate affected by delamination. The crustal thickness of the SE margin of Tibet is about 60 km beneath SGT, thinning to 42 km in the east direction, and reaching a low value of 34 km beneath Simao city in the south. The variation in crustal thickness is distinct, changing sharply beneath Longmenshan Mountain, and much smoother in the south direction, and the middle-lower ductile layer also thins distinctly, which we speculate that it is related to the lower crustal flow from Tibetan Plateau to the Indochina block, after encountering the rigid Yangtze craton during the Cenozoic period.

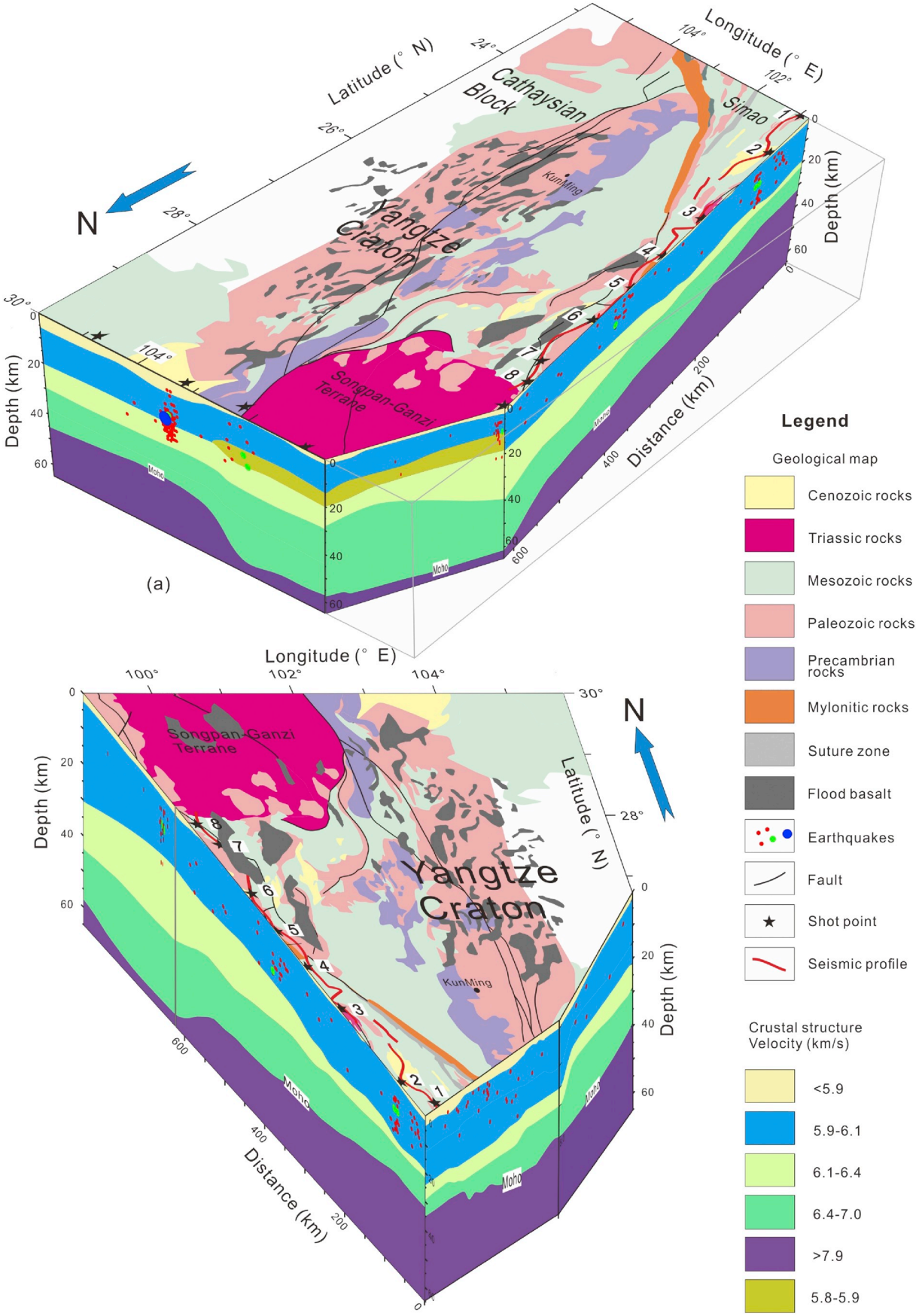

Fig. 15. Three-dimensional perspective view of the crustal velocity structure along profiles: (a) Zhubalong-Zizhong (Line 11 in Fig. 1) [Wang et al., 2007], Benzilan-Tangke (Line10 in Fig. 1) [Wang et al., 2007] and our profile; (b) our profile and Puer-Luxi (Line 6 in Fig. 1) (Zhang et al., 2013a). The dots represent the distribution of seismic events occurred during the period of 2008.01–2018.01 less than 40 km from each profile. The red dots show a magnitude of 3.0–5.0, the green dots represent a magnitude of 5.0–7.0, and the blue dots indicate a magnitude larger than 7.0;

Acknowledgements

We gratefully acknowledge Prof. Chunyong Wang for providing the DSS data from "Dian-Shen 8687" project. We thank Dr. G. F. Viejo and an anonymous reviewer for their constructive comments and suggestions for the manuscript. This work is supported by the DREAM project of the National Key R&D Program of China (2016YFC0600402), the National Key Research and Development Project of China (2016YFC0600302), the National Natural Science Foundation of China (41774071, 41774072, 41522401, 41774097, 41574084), and China Earthquake Science Experiment (2016CESE0103). We used the GMT software package (Wessel and Smith, 1998) for production of some figures.

References

Akciz, S., Burchfiel, B.C., Crowley, J.L., Yin, J., Chen, L., 2008. Geometry, kinematics, and regional significance of the Chong Shan shear zone, Eastern Himalayan Syntaxis, Yunnan, China. Geosphere 4 (1), 292–314.

Bai, Z., Wang, C., 2003. Tomographic investigation of the upper crustal structure and seismotectonic environments in Yunan province. Acta Seismol. Sin. 25 (2), 117–127 (in Chinese).

Bai, D., Unsworth, M.J., Meju, M.A., Ma, X., Teng, J., Kong, X., Sun, Y., Sun, J., Wang, L., Jiang, C., Zhao, C., Xiao, P., Liu, M., 2010a. Crustal deformation of the eastern Tibetan plateau revealed by magnetotelluric imaging. Nature 3, 358–362.

Bai, L., Tian, X., Ritsema, J., 2010b. Crustal structure beneath the Indochina peninsula from teleseismic receiver functions. Geophys. Res. Lett. 37, L24308.

Braile, L.W., Smith, R.B., 1975. Guide to the interpretation of crustal refraction profiles. Geophys. J. R. Astron. Soc. 40, 145–176.

Calais, E., Dong, L., Wang, M., Shen, Z., Vergnolle, M., 2006. Continental deformation in Asia from a combined GPS solution. Geophys. Res. Lett. 33, L24319. https://doi.org/10.1029/2006GL028433.

Cerveny, V., Psencik, I., 1984. SEIS83-numerical modeling of seismic wavefield in 2-D laterally varying layered structures by the ray method. In: Engdahl, E.R. (Ed.), Documentation of Earthquake Algorithm. World Data Center for Solid Earth Geophys., Boulder, Colo., pp. 36–40.

Cerveny, V., Molotkov, I.A., Psencik, I. (Eds.), 1977. Ray Method in Seismology. Univ. Karlova, Prague, pp. 57–158.

Chen, Y., Niu, F., Liu, R., Huang, Z., Tkalčić, H., Sun, L., Chan, W., 2010. Crustal structure beneath China from receiver function analysis. J. Geophys. Res. 115, B03307.

Chen, Y., Zhang, Z., Sun, C., Badal, J., 2013. Crustal anisotropy from Mono converted Ps wave splitting analysis and geodynamic implications beneath the eastern margin of Tibet and surrounding regions. Gondwana Res. 24, 946–957.

Chen, S., Wang, B., Tian, X., Wang, F., Liu, B., Li, L., 2016. Crustal structure from Yunxian-Ninglang wide-angle seismic reflection and refraction profile in northwestern Yunan, China. Seismol. Geol. 38, 91–106 (in Chinese).

Christensen, N.I., Mooney, W.D., 1995. Seismic velocity structure and composition of the continental crust: a global view. J. Geophys. Res. 100 (B7), 9761–9788.

Clark, M.K., Royden, L.H., 2000. Topographic ooze: building the eastern margin of Tibet by lower crustal flow. Geology 28, 703–706.

Deng, J., Wang, Q., Li, G., Li, C., Wang, C., 2014a. Tethys tectonic evolution and its bearing on the distribution of important mineral deposits in the Sanjiang region, SW China. Gondwana Res. 26, 419–437.

Deng, J., Wang, Q., Li, G., Santosh, M., 2014b. Cenozoic tectono-magmatic and metallogenic processes in the Sanjiang region, southwestern China. Earth Sci. Rev. 138, 268–299.

England, P., Houseman, G., 1986. Finite strain calculations of continental deformation 2. Comparison with the India-Asia collision zone. J. Geophys. Res. 91 (B3), 3664–3676.

Enkelmann, E., Ratschbacher, L., Jonckheere, R., Nestler, R., Fleischer, M., Gloaguen, R., Hacker, B.R., Zhang, Y.Q., Ma, Y.S., 2006. Cenozoic exhumation and deformation of northeastern Tibet and the Qinling: is Tibetan lower crustal flow diverging around the Sichuan basin? GSA Bull. 118, 651–671.

Enkelmann, E., Weislogel, A., Ratschbacher, L., Eide, E., Renno, A., Wooden, J., 2007. How was the Triassic Songpan-Ganzi basin filled? A provenance study. Tectonics 26, TC4007. https://doi.org/10.1029/2006TC002078.

Fu, Y.V., Gao, Y., Li, A., Li, L., Chen, A., 2017. Lithospheric structure of the southeastern margin of the Tibetan Plateau from Rayleigh wave tomography. J. Geophys. Res. Solid Earth 122, 4631–4644.

Fuchs, K., Muller, G., 1971. Computation of synthetic seismograms with the reflectivity method and comparison with observations. Geophys. J. Astr. Soc. 23, 417–433.

Gao, S., Rudnick, R.L., Carlson, R.W., McDonough, W.F., Liu, Y., 2002. Re-Os evidence for replacement of ancient mantle lithosphere beneath the North China craton. Earth Planet. Sci. Lett. 198, 307–322.

Giese, P., Prodehl, C., Stein, A. (Eds.), 1976. Explosion Seismology in Central Europe. Springer-Verlag, New York, pp. 146–161.

Grad, M., Jensen, S.L., Keller, G.R., Guterch, A., Thybo, H., Janik, T., Tiira, T., Yliniemi, J., Luosto, U., Motuza, G., Nasedkin, V., Czuba, W., Gaczyński, E., Środa, P., Miller, K.C., Wilde-Piórko, M., Komminaho, K., Jacyna, J., Korabliova, L., 2003. Crustal structure of the Trans-European suture zone region along POLONAISE'97 seismic profile P4. J. Geophys. Res. 108 (B11), 2541.

He, B., Xu, Y.G., Chung, S.L., Xiao, L., Wang, Y., 2003. Sedimentary evidence for a rapid, kilometer-scale crustal doming prior to the eruption of the Emeishan flood basalts. Earth Planet. Sci. Lett. 213, 391–405.

Hole, J.A., 1992. Nonlinear high-resolution three-dimensional seismic travel time tomography. J. Geophys. Res. 97, 6553–6562.

Hu, S., He, L., Wang, J., 2000. Heat flow in the continental area of China: a new data set. Earth Planet. Sci. Lett. 179, 407–419.

Huang, Z., Wang, L., Xu, M., Liu, J., Mi, N., Liu, S., 2007. Shear wave splitting across the Ailao Shan-Red River fault zone, SW China. Geophys. Res. Lett. 34, L20301. https://doi.org/10.1029/2007GL031236.

Huang, H., Yao, H., van der Hilst, R.D., 2010. Radial anisotropy in the crust of SE Tibet and SW China from ambient noise interferometry. Geophys. Res. Lett. 37, L21310. https://doi.org/10.1029/2010GL044981.

Jia, S., Liu, B., Xu, Z., Liu, Z., Feng, S., Zhang, J., Lin, J., Tian, X., Liu, Q., Guo, W., 2014a. The crustal structure of the central Longmenshan along and its margins as related to the seismotectonics of the 2008 Wenchuan Earthquake. Sci. China Earth Sci. 57, 777–790.

Jia, S., Wang, F., Tian, X., Duan, Y., Zhang, J., Liu, B., Lin, J., 2014b. Crustal structure and tectonic study of North China craton from a long deep seismic sounding profile. Tectonophysics 627, 48–56.

Kan, R., Hu, H., Zeng, R., Mooney, W.D., McEvilly, T.V., 1986. Crustal structure of Yunan province, People's Republic of China, from seismic refraction profiles. Science 234, 433–437.

Lei, J., Zhao, D., Su, Y., 2009. Insight into the origin of the Tengchong intraplate volcano and seismotectonics in southwest China from local and teleseismic data. J. Geophys. Res. 114, B05302.

Lei, J., Li, Y., Xie, F., Teng, J., Zhang, G., Sun, C., Zha, X., 2014. Pn anisotropic tomography and dynamics under eastern Tibetan plateau. J. Geophys. Res. Solid Earth 119, 2174–2198. https://doi.org/10.1002/2013JB010847.

Li, X., Zhu, P., Kusky, T.M., Gu, Y., Peng, S., Yuan, Y., Fu, J., 2015. Has the Yangtze craton lost its root? A comparison between the North China and Yangtze cratons. Tectonophysics 655, 1–14.

Li, J., Song, X., Zhu, L., Deng, Y., 2017. Joint inversion of surface wave dispersions and receiver functions with P velocity constraints: Application to southeastern Tibet. J. Geophys. Res. Solid Earth 122, 7291–7310.

Lin, Z., Hu, H., Zhang, W., Zhang, H., He, Z., Lin, Z., Qiu, T., 1993. Preliminary interpretation of a deep seismic sounding in Western Yunan. Acta Seismol. Sin. 15, 427–440 (in Chinese).

Liu, M., Mooney, W.D., Li, S., Okaya, N., Detweiler, S., 2006. Crustal structure of the northeastern margin of the Tibetan plateau from the Songpan-Ganzi terrane to the Ordos basin. Tectonophysics 420, 253–266.

Liu, Q.Y., Hilst, R.D., Li, Y., Yao, H.J., Chen, J.H., Guo, B., Qi, S.H., Wang, J., Huang, H., Li, S.C., 2014. Eastward expansion of the Tibetan Plateau by crustal flow and strain partitioning across faults. Nature 7, 361–365.

Ma, L., 2002. Atlas of Chinese Geology. Geological Publishing House, Beijing, pp. 293–300 (In Chinese).

Royden, L.H., Burchfiel, B.C., King, R.W., Wang, E., Chen, Z., Shen, F., Liu, Y., 1997. Surface deformation and lower crustal flow in eastern Tibet. Science 276, 788–790.

Royden, L.H., Burchfiel, B.C., Hilst, R.D., 2008. The geological evolution of the Tibetan Plateau. Science 321, 1054–1058.

Shen, Z.K., Lü, J., Wang, M., Bürgmann, R., 2005. Contemporary crustal deformation around the southeast borderland of the Tibetan Plateau. J. Geophys. Res. 110, B11409. https://doi.org/10.1029/2004JB003421.

Song, X.Y., Zhou, M.F., Cao, Z.M., Robinson, P.T., 2004. Late Permian rifting of the south China craton caused by the Emeishan mantle plume? J. Geol. Soc. Lond. 161, 773–781.

Steckler, M.S., Mondal, D.R., Akhter, S.H., Seeber, L., Feng, L., Gale, J., Hill, E.M., Howe, M., 2016. Locked and loading megathrust linked to active subduction beneath the Indo-Burman Ranges. Nature 9, 615–618.

Sun, X., Bao, X., Xu, M., Eaton, D.W., Song, X., Wang, L., Ding, Z., Mi, N., Yu, D., Li, H., 2014. Crustal structure beneath SE Tibet from joint analysis of receiver functions and Rayleigh wave dispersion. Geophys. Res. Lett. 41, 1479–1484.

Tapponnier, P., Peltzer, G., Le Dain, A.Y., Armijo, R., 1982. Propagating extrusion tectonics in Asia: New insights from simple experiments with plasticine. Geology 10, 611–616.

Tapponnier, P., Xu, Z., Roger, F., Meyer, B., Arnaud, N., Wittlinger, G., Yang, J., 2001. Oblique stepwise rise and growth of the Tibet Plateau. Science 294, 1671–1677.

Vidale, J.E., 1988. Finite-difference calculation of travel times. Bull. Seismol. Soc. Am. 78, 2062–2076.

Vidale, J.E., 1990. Finite-difference calculation of traveltimes in three dimensions. Geophysics 55, 521–526.

Wang, Y., 2001. Heat flow pattern and lateral variations of lithosphere strength in China mainland: constraints on active deformation. Phys. Earth Planet. Inter. 126, 121–146.

Wang, C., Han, W., Wu, J., Lou, H., Chan, W.W., 2007. Crustal structure beneath the eastern margin of the Tibetan Plateau and its tectonic implications. J. Geophys. Res. Solid Earth 112, B07307.

Wang, C., Lou, H., Wang, X., Qin, J., Yang, R., Zhao, J., 2009. Crustal structure in Xiaojiang fault zone and its vicinity. Earthq. Sci. 22, 347–356.

Wang, C., Zhu, L., Lou, H., Huang, B., Yao, Z., Luo, X., 2010. Crustal thickness and Poisson's ratios in the eastern Tibetan Plateau and their tectonic implications. J. Geophys. Res. Solid Earth 115, B11301.

Wang, Y., Mooney, W.D., Yuan, X., Okaya, N., 2013. Crustal structure of the Northeastern Tibetan Plateau from the southern Tarim Basin to the Sichuan Basin, China. Tectonophysics 584, 191–208.

Wang, F., Pan, S., Liu, L., Liu, B., Zhang, J., Deng, X., Ma, C., Zhang, C., 2014a. Wide angle seismic exploration of Yuxi-Lincang profile-the research of crustal structure of the red river fault zone and southern Yunnan. Chin. J. Geophys. 57, 3247–3258 (in Chinese).

Wang, W., Wu, J., Fang, L., Lai, G., Yang, T., Cai, Y., 2014b. S wave velocity structure in southwest China from surface wave tomography and receiver functions. J. Geophys. Res. Solid Earth 119, 1061–1078.
Wang, S., Liu, B., Zhang, J., Liu, B., Duan, Y., Song, X., Deng, X., Ma, C., Zang, Y., 2015. Study on the velocity structure of the crust in Southwest Yunnan of the north-south seismic belt-results from the Menghai-Gengma-Lushui deep seismic sounding profile. Sci. China Earth Sci. 58, 2175–2187 (in Chinese).
Wang, W., Wu, J., Fang, L., Lai, G., Cai, Y., 2017. Crustal thickness and Poisson's ratio in southwest China based on data from dense seismic arrays. J. Geophys. Res. Solid Earth 122, 7219–7235. https://doi.org/10.1002/2017JB013978.
Wessel, P., Smith, W., 1998. New, improved version of Generic Mapping Tools released. Eos. Trans. AGU 79, 579.
Xu, Y., Chung, S.L., Jahn, B., Wu, G., 2001. Petrologic and geochemical constraints on the petrogenesis of Permian-Triassic Emeishan flood basalts in southwestern China. Lithos 58, 145–168.
Xu, T., Zhang, Z., Liu, B., Chen, Y., Zhang, M., Tian, X., Xu, Y., Teng, J., 2015. Crustal velocity structure in the Emeishan large igneous province and evidence of the Permian mantle plume activity. Sci. China Earth Sci. 58 (7), 1133–1147.
Yin, A., Harrison, T.M., 2000. Geologic evolution of the Himalayan-Tibetan orogen. Annu. Rev. Earth Planet. Sci. 28, 211–280.
Yu, Y., Gao, S.S., Liu, K.H., Yang, T., Xue, M., Le, K.P., 2017. Mantle transition zone discontinuities beneath the Indochina Peninsula: implications for slab subduction and mantle upwelling. Geophys. Res. Lett. 44, 7159–7167.
Zhai, M., Fan, Q., Zhang, H., Sui, J., Shao, J., 2007. Lower crustal processes leading to Mesozoic lithospheric thinning beneath eastern North China: underplating, replacement and delamination. Lithos 96, 36–54.
Zhang, X., Wang, Y., 2009. Crustal and upper mantle velocity structure in Yunnan, Southwest China. Tectonophysics 471, 171–185.
Zhang, P., Shen, Z., Wang, M., Gan, W., Bürgmann, R., Molnar, P., Wang, Q., Niu, Z., Sun, J., Wu, J., Sun, H., You, X., 2004. Continuous deformation of the Tibetan Plateau from global positioning system data. Geology 32, 809–812.
Zhang, Z., Zhao, B., Zhang, X., Liu, C., 2006. Crustal structure beneath the wide-angle seismic profile between Simao and Zhongdian in Yunan. Chin. J. Geophys. 49 (5), 1377–1384 (in Chinese).
Zhang, H., Parrish, R., Zhang, L., Xu, W., Yuan, H., Gao, S., Crowley, Q., 2007. A-type granite and adakitic magmatism association in Songpan-Garze fold belt, eastern Tibetan Plateau: implication for lithosphere delamination. Lithos 97, 323–335.
Zhang, Z., Bai, Z., Mooney, W.D., Wang, C., Chen, X., Wang, E., Teng, J., Okaya, N., 2009. Crustal structure across the Three Gorges area of the Yangtze platform, central China, from seismic refraction/wide-angle reflection data. Tectonophysics 475, 423–437.
Zhang, E., Lou, H., Jia, S., Li, Y., 2013a. The deep crust structure characteristics beneath western Yunan. Chin. J. Geophys. 56, 1915–1927 (in Chinese).
Zhang, Z., Xu, T., Zhao, B., Badal, J., 2013b. Systematic variations in seismic velocity and reflection in the crust of Cathaysia: new constraints on intraplate orogeny in the South China continent. Gondwana Res. 24, 902–917.
Zhang, R., Wu, Y., Gao, Z., Fu, Y.V., Sun, L., Wu, Q., Ding, Z., 2017. Upper mantle discontinuity structure beneath eastern and southeastern Tibet: new constraints on the Tengchong intraplate volcano and signatures of detached lithosphere under the western Yangtze Craton. J. Geophys. Res. Solid Earth 122, 1367–1380.
Zhao, L., Xie, X., He, J., Tian, X., Yao, Z., 2013. Crustal flow pattern beneath the Tibetan Plateau constrained by regional Lg-wave Q tomography. Earth Planet. Sci. Lett. 383, 113–122.
Zheng, J., Griffin, W.L., O'Reilly, S.Y., Zhang, M., Pearson, N., Pan, Y., 2006. Widespread Archean basement beneath the Yangtze craton. Geology 34 (6), 417–420.
Zheng, D., Saygin, E., Cummins, P., Ge, Z., Min, Z., Cipta, A., Yang, R., 2017. Transdimensional Bayesian seismic ambient noise tomography across SE Tibet. J. Asia Earth Sci. 134, 86–93.
Zhu, B.Q., Mao, C.X., Lin, G.W., Mccdougall, J.D., 1983. Isotopic and geochemical evidence for the origin of Plio-Pleistocene volcanic rocks near the Indo-Eurasian collisional margin at Tengchong, China. Earth Planet. Sci. Lett. 65, 263–275.
Zhu, M., Graham, S., Mchargue, T., 2009. The Red River Fault zone in the Yinggehai Basin, South China Sea. Tectonophysics 476, 397–417.